ELSEVIER

Physics of the Earth and Planetary Interiors 109 (1998) 25–63

PHYSICS OF THE EARTH AND PLANETARY INTERIORS

Deep earthquakes beneath the Fiji Basin, SW Pacific: Earth's most intense deep seismicity in stagnant slabs

Emile A. Okal [a,*], Stephen H. Kirby [b]

[a] *Department of Geological Sciences, Northwestern University, Evanston, IL 60208, USA*
[b] *United States Geological Survey, 345 Middlefield Road, Menlo Park, CA 94025, USA*

Received 13 February 1998; revised 19 June 1998; accepted 24 June 1998

Abstract

Previous work has suggested that many of the deep earthquakes beneath the Fiji Basin occur in slab material that has been detached and foundered to the bottom of the transition zone or has been laid down by trench migration in a similar recumbent position. Since nowhere else in the Earth do so many earthquakes occur in slabs stagnated in the transition zone, these earthquakes merit closer study. Accordingly, we have assembled from historical and modern data a comprehensive catalogue of the relocated hypocenters and focal mechanisms of well-located deep events in the geographic area between the bottoms of the main Vanuatu and Tonga Wadati–Benioff zones. Two regions of deep seismogenesis are recognized there: (i) 163 deep shocks have occurred north of 15°S in the Vityaz Group from 1949 to 1996. These seismological observations and the absence of other features characteristic of active subduction suggest that the Vityaz group represents deep failure in a detached slab that has foundered to a horizontal orientation near the bottom of the transition zone. (ii) Another group of nearly 50 'outboard' deep shocks occur between about 450 and 660 km depth, west of the complexly buckled and offset western edge of the Tonga Wadati–Benioff zone. Their geometry is in the form of two or possibly three small-circle arcs that roughly parallel the inferred motion of Tonga trench migration. Earthquakes in the southernmost of these arcs occur in a recumbent high-seismic-wavespeed slab anomaly that connects both to the main inclined Tonga anomaly to the east and a lower mantle anomaly to the west [Van der Hilst, R., 1995. Complex morphology of subducted lithosphere in the mantle beneath the Tonga trench. Nature, Vol. 374, pp. 154–157.]. Both groups show complexity in their focal mechanisms. The major question raised by these observations is the cause of this apparent temporary arrest in the descent of the Tonga slab into the lower mantle. We approach these questions by considering the effects of buoyant metastable peridotite in cold slab material that was detached and rapidly foundered, or was buckled, segmented and laid out in the transition zone.

Keywords: Deep earthquakes; Fiji Basin; Slabs

1. Introduction and background

The principal geography of the Earth's seismicity below 300 km depth was established during the first 60 years of global instrumental seismology (Gutenberg and Richter, 1938, 1939, 1949) However, at least four zones of deep activity escaped detection in these pioneering studies: the large Spanish deep earthquake of 29 March 1954 and its subsequent small companions (Chung and Kanamori, 1976; Buforn et al., 1991); the zone of deep shocks beneath

* Corresponding author. Tel.: +1-8474913741; Fax: +1-8474918060

0031-9201/98/$ - see front matter
PII: S0031-9201(98)00116-2

New Zealand (Adams, 1963; Adams and Ferris, 1976; Anderson and Webb, 1994); the deep seismic zone beneath the Tyrrhenian Sea in the Western Mediterranean (Peterschmitt, 1956; Anderson and Jackson, 1987; Giardini and Velonà, 1991; Frepoli et al., 1996); and finally, the region with the highest recent activity beneath the North and South Fiji Basins between the Tonga and Vanuatu Wadati–Benioff Zones [WBZ] (Sykes, 1964; Isacks et al., 1967; Isacks and Molnar, 1971; Barazangi et al., 1973; Hamburger and Isacks, 1987). These blanks in the early catalogues of deep events may well reflect the large magnitude detection thresholds that generally existed before the modern era and the relatively small magnitudes typical of modern events in those regions (except the large 1954 Spanish earthquake). Improvements in seismic instrumentation in the late 1950s and 1960s provided better station coverage and lower detection thresholds, especially for the southern hemisphere, resulting in discovery of these new regions of deep activity.

In most of these examples, large depth gaps exist between the deep zones and nearby intermediate-depth seismicity when the latter is present. These depth gaps and other seismic data have fueled discussion of whether deep seismogenic material is mechanically detached from the lithosphere currently entering nearby trenches or is continuous slab material that is merely aseismic (Isacks et al., 1968; Sacks, 1969; Isacks and Molnar, 1971; Barazangi et al., 1973; Hamburger and Isacks, 1987; James and Snoke, 1990; Buforn et al., 1991; Engdahl et al., 1995; Okal et al., 1995; Okal and Talandier, 1997).

Another class of anomalous deep earthquakes are those that occur above the main WBZ or above its along-dip projection into the lower mantle (see review by Lundgren and Giardini, 1994). Such 'outboard' events occur typically at depths of less than 600 km and most are 60 to 160 km shallower than the 660 km discontinuity defining the bottom of the transition zone, an important observation discussed later. Outboard events are usually sparse in deep WBZs. There are two exceptions to this generalization. One is the deep seismic zone of eastern Indonesia east of longitude 120°E and especially the segment between 120 and 126°E, where a score of historical and modern outboard deep earthquakes are documented up to 1995, well north of, and generally shallower than, the bottom of the steeply-dipping and E–W-trending Indonesian WBZ near latitude 6.8°S. However, many unusual features of the plate boundary complicate the interpretation and identification of slab provenance for outboard deep shocks in this region. The second exception is the zone of deep activity west of the main Tonga WBZ between 17 and 22°S. Four dozen deep shocks have occurred in that region since 1963, making it the most active region of outboard deep seismicity in the Earth's interior.

Recent tomographic images of the source regions of outboard earthquakes indicate that they occur in flat-lying, high-wavespeed anomalies that are more or less continuous with the bottom of the main WBZ nearby (Zhou, 1988; Fukao et al., 1992; Van der Hilst et al., 1991, 1993; Van der Hilst and Seno, 1993; Engdahl et al., 1995; Van der Hilst, 1995; Widiyantoro and Van der Hilst, 1996). Also, the focal mechanisms of these shocks tend to be different from those in the main zone (Lundgren and Giardini, 1994). These studies suggest that slabs can become recumbent by somehow stagnating in the transition zone of the mantle. Thus, earthquakes in both detached and outboard settings may represent deep seismic failure in stagnated slab material.

Routine reports of deep events beneath the North Fiji Basin first appeared in the bulletins of the Bureau Central International de Séismologie [BCIS], the International Seismological Summary [ISS], and the US Coast and Geodetic Survey in the late 1950s and early 1960s. Sykes (1964) first pointed out the significance of the deep events beneath the North Fiji Basin, noting that they seemed to have greater affinity to the WNW trends of eastern Melanesian arcs and the Vityaz trench than to the Tonga–Kermadec or Vanuatu (New Hebrides) arcs. Many outboard events have also occurred more recently west of Tonga, above the down-dip continuation of the main Tonga zones (e.g., Giardini and Woodhouse, 1984).

Hamburger and Isacks (1987) reviewed the geological and geophysical evidence that suggested that the deep Fiji Basin events do not reflect the present-day Tonga/Kermadec and Vanuatu subduction geometry. Instead, they concluded that such earthquakes represent failure in deep detached and/or foundered slabs created by arc reversal at the fossil

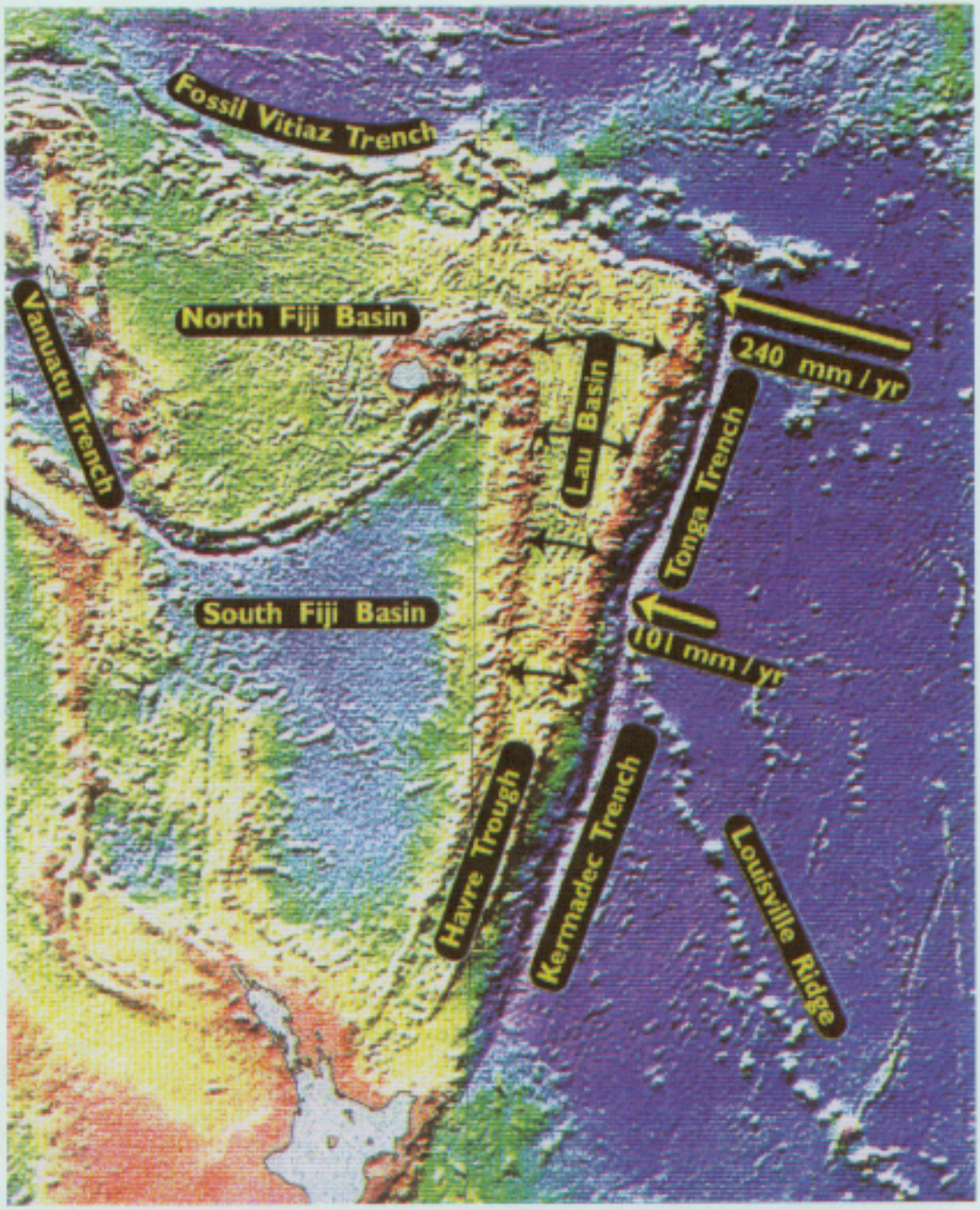

Fig. 1. Tectonic setting of the region between the Tonga/Vanuatu/Vityaz trenches (SW Pacific) featuring a complex history of arc reversal, slab detachment, back-arc extension and rapid trench migration and rotation in the Late Cenozoic. Color shaded relief map from the global bathymetric map of Smith and Sandwell (1997). Plate motion vectors from GPS observations of Bevis et al. (1995) and from the model of McCaffrey (1994).

Vityaz arc and rapid trench migration, and associated back-arc spreading occurring behind the Tonga and Vanuatu subduction zones in the latest Cenozoic (Fig. 1). Van der Hilst (1995) has shown that many of the outboard events west of the main Tonga zone occur in flat-lying, high-seismic wavespeed material that is continuous with the inclined Tonga slab. He also showed that west of this region of recumbent slab material, a high-wavespeed anomaly is found in the lower mantle. Van der Hilst relates this complex slab morphology to the Late Cenozoic history of trench migration in the Tonga subduction zone, an evolutionary model that we discuss later in this paper.

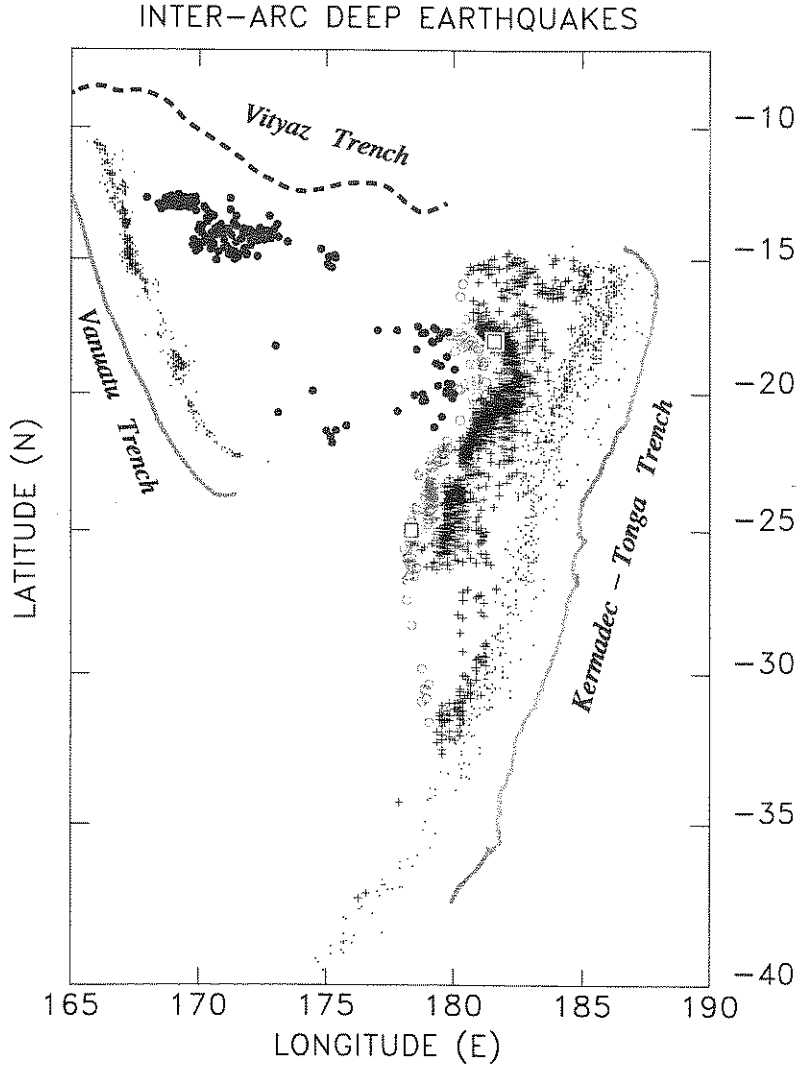

Fig. 2. Regional map of the epicenters of the 211 deep earthquakes that have occurred during 1949–1996 in the inter-arc region between the Tonga, Vanuatu and Vityaz subduction zones (filled circles). Events were relocated as described in the text. The background seismicity at depths greater than 100 km is also shown, based on relocations by Engdahl et al. (1997): the smaller symbols are for the 100–300 km depth band and the + signs for events deeper than 300 km. The outboard earthquakes, offset and isolated from the bottom of the seismic zone, are shown as open circles. The two open squares are the large events of 1994 (to the North) and 1932 (to the South; Okal, 1997). Note the Vityaz group of earthquakes and the finger shaped events west of the northern Tonga subduction zone.

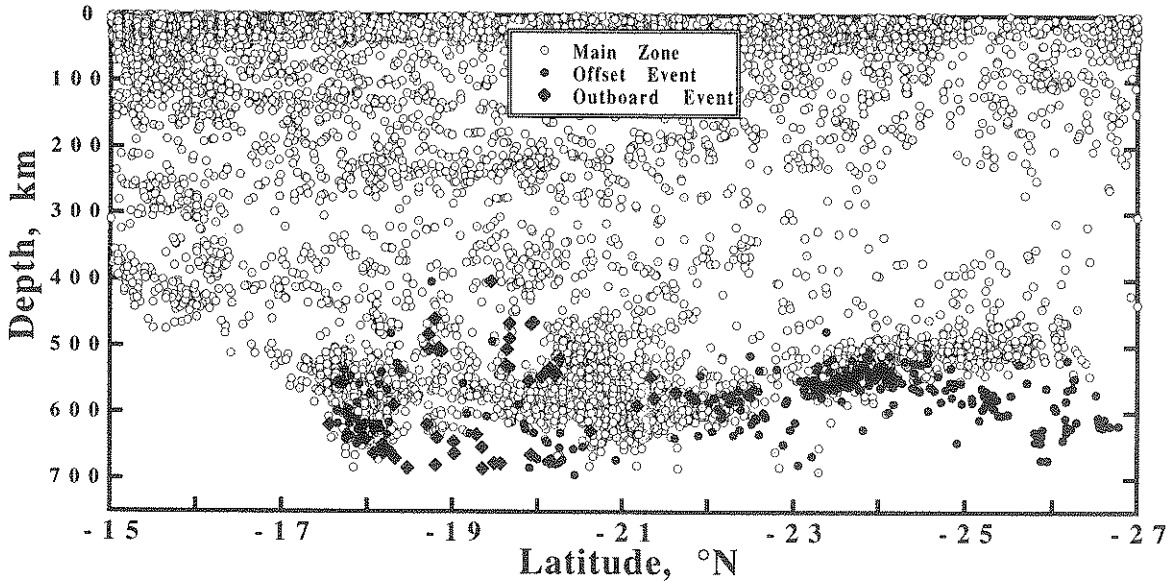

Fig. 3. North–south cross section through the Tonga Wadati–Benioff Zone (WBZ). Note the complex geometry of the bottom of the seismic zone, especially where there are deep gaps, such as the one between latitudes 18 and 20°S. From the catalogue of Engdahl et al. (1997) covering the period 1964 through 1995.

These unusual deep events beneath the Fiji Basin (Figs. 2 and 3) present a unique opportunity. Nowhere else have so many deep earthquakes occurred in stagnant slab material evidently detached from currently active subduction or in recumbent slab material that is above the down-dip projection of a main WBZ. Their occurrence poses a significant problem as to why earthquakes occur at all in stagnated and foundered material. Such slab material is evidently no longer rapidly sinking and has no column of denser slab material compressing it from above. Actively descending slabs that are continuous with surface oceanic plates can develop appreciable stresses by the summation of buoyancy forces in the slab stress guide, generally in equilibrium with viscous forces (e.g., Vassiliou and Hager, 1988). This is thought to be the primary origin of down-dip P axes of deep earthquakes in WBZs (Isacks et al., 1968; Isacks and Molnar, 1969, 1971; Richter, 1979). Given the likelihood that the forces producing these slab stresses are minimal in recumbent stagnant slabs, what is the origin of stresses in such settings? Moreover, by what failure process can deep earthquake faulting occur?

The deep earthquakes beneath the Fiji Basin and Plateau thus provide us with an opportunity to study seismogenic failure in slabs that have foundered and stagnated in the transition zone and hence to make inferences about their internal thermophysical conditions. The plan of this paper is to: (i) provide a comprehensive summary of the instrumental record of deep earthquake activity in the Fiji Basin occurring outside the main Vanuatu and Tonga slab systems by creating a catalogue of deep events relocated by a modern uniform methodology and by reviewing published and new focal mechanisms; (ii) examine the fine structure and deformation geometries of these deep zones using these data; and (iii) discuss these findings in light of the regional seismo-tectonic setting and recent hypotheses of the mineralogy of deep slabs and the physics of deep earthquakes.

2. Methods

2.1. Selection of data

We used the NEIC computerized files to extract all earthquakes reported in the area covered by

Fig. 4, regardless of depth, and for the time window January 1920–June 1996 ('the database'). The irregular polygon ('the box') delineates a region in which deep and/or intermediate-depth seismicity (those earthquakes with a depth $h \geq 200$ km) cannot be related to well-documented WBZs, or involves clear outliers to these zones. Outside the box, we use smaller symbols to plot unrelocated deep solutions ($h \geq 200$ km) obtained from the database for the years 1963–1996. Larger symbols are used to plot the relocated epicenters of events whose original locations lay inside the box.

The events targeted for examination and relocation consist of the following.

(i) All events from the database for the years 1963–1996, for which initial locations fall inside the box and have $h \geq 200$ km.

(ii) Those database events for the years 1920–1962 for which $h \geq 200$ km, with initial locations inside the box and west of 178°E. (East of 178°E, the

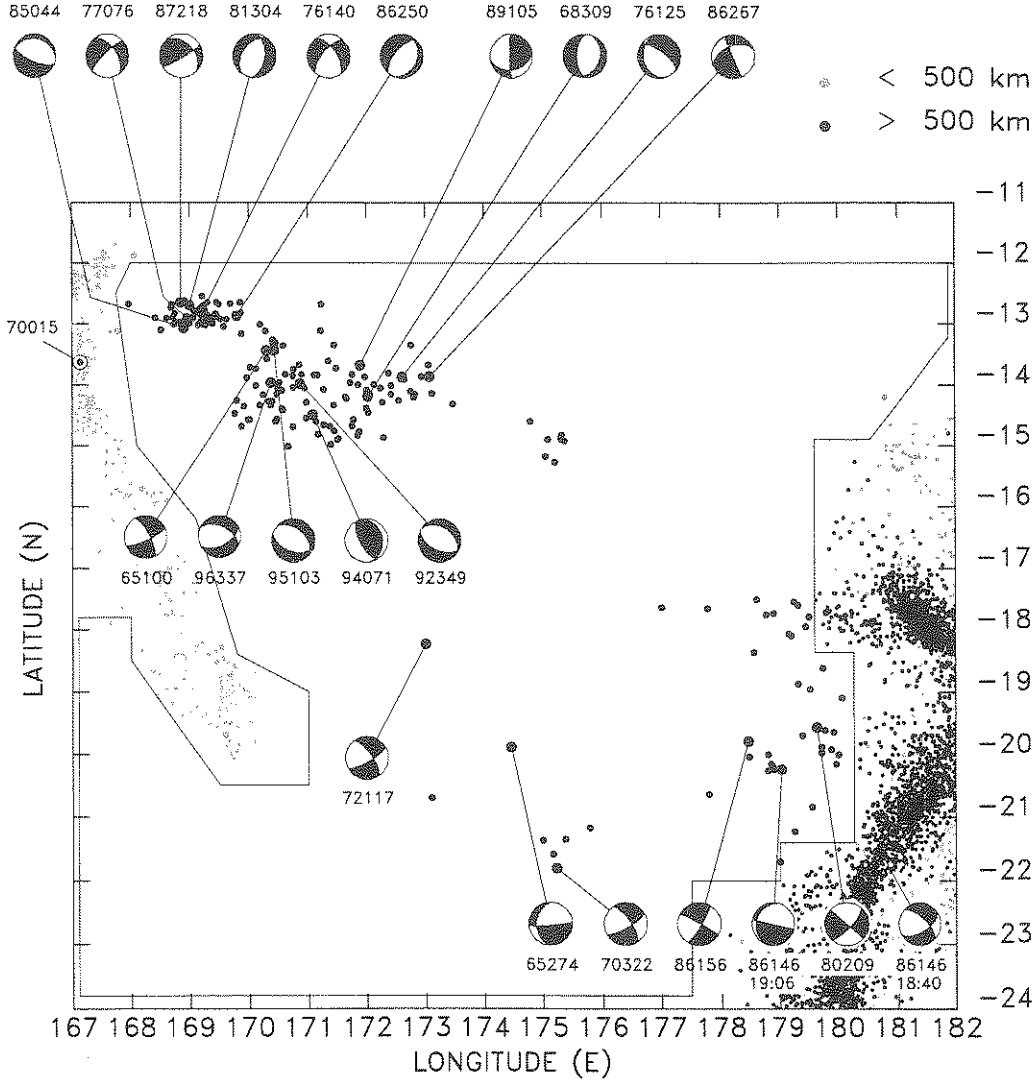

Fig. 4. Area of detailed study. The smaller symbols outside the irregular box are unrelocated deep earthquakes ($h \geq 200$ km) compiled from the NEIC catalogue for 1963–1996. All earthquakes inside the box are the final relocations compiled in Tables 1 and 2. Note the event (70015) below the Vanuatu WBZ. All focal mechanisms listed in Table 5 are also shown, with corresponding Julian dates.

inclusion of historical earthquakes would have required the relocation of a major part of the catalogue of Tonga–Fiji historical events, an effort beyond the scope of this study.)

(iii) Since the shallow seismicity in the Fiji Basin, largely associated with complex back-arc spreading, has been studied extensively (e.g., Hamburger and Isacks, 1987; Chen and Grimison, 1989), it will generally not be discussed here. However, we targeted for relocation any events with anomalously large reported depths ($h \geq 50$ km) initially located inside the Fiji Basin (that section of the box west of 178°E, and excluding the Vanuatu WBZ).

(iv) Finally, under the North Fiji Basin (that section of the box north of 15.5°S and west of 177°E), we relocated all shallower earthquakes (0–50 km; 1920–1996), in order to investigate whether any intermediate-depth seismicity could be found between the Vityaz cluster and the Vityaz Trench. Incidentally, this effort revealed three historical earthquakes (one in 1949 and two in 1958) initially reported as shallow, but clearly relocating into the deep Vityaz cluster. As will be discussed one intermediate depth event was also possibly identified.

Hypocentral solutions and arrival time data were examined for a total of 414 earthquakes

2.2. Relocation procedure

The general approach and algorithm of the relocation effort follow the steps described in Wysession et al. (1991), including Monte Carlo tests of the precision of the solution conducted by injecting noise into the dataset of arrival times. For each targeted earthquake, we extracted its ISS/ISC entry (BCIS during the lean years of the ISS (1956–1963)). Historical earthquakes (pre-1963) were systematically relocated. For post-1963 events, the ISC epicenter was retained if: a minimum of 10 stations were used in the ISC location; AND a root-mean-squares residual of less than 2 s was achieved; AND no pattern of aberrant residuals was present. In many instances, the precision of the retained ISC locations were examined using the Monte Carlo test. For events after June 1995, lacking ISC locations, PDE locations were retained.

Extreme and irregular delays of S waves in the Fiji Basin area have been reported (e.g., Frohlich and Barazangi, 1980), and thus S arrival times were generally not used. Nevertheless, because we used a uniform and objective method for historical relocations, evaluated the importance of each datum (Minster et al., 1974), and subjected the resulting solutions to Monte Carlo tests, we believe that our procedure improves the quality of our hypocenters compared to the original bulletin locations.

3. Results

The larger symbols on Fig. 4 show our relocated epicenters ($h \geq 200$ km). With the exception of a few events which remain as possible outliers to the Fiji–Tonga WBZ, all earthquakes relocate either in the deep Vityaz cluster, or in the South Fiji Basin zone of deep scattered seismicity, or into the main bodies of the Vanuatu and Tonga–Fiji WBZs. The final compilation of the seismicity is given in Tables 1 and 2. Table 3 lists casualties of the relocation, i.e., events relocating outside of the Vityaz and deep Fiji clusters.

These results clearly indicate that the Vityaz cluster is spatially isolated from the Tonga WBZ: the few deep events with epicenters originally between 178°E and 179°W, at 14–15°S, which would have suggested a possible zone of continuous, diffuse seismicity between the Vityaz cluster and the Tonga WBZ, all relocate into the latter. Similarly, the events originally located at intermediate depths between the Vanuatu WBZ and the South Fiji Basin deep seismic zone, relocate into the Vanuatu slab. As a result, the deep seismicity in our study area, as defined by the box on Fig. 4, can be separated into a number of well-defined entities which we describe in detail below.

3.1. The Vityaz cluster

Fig. 5 is a close-up of the Vityaz cluster, a group of 163 deep earthquakes whose relocated parameters are listed in Table 1. We subdivide the cluster into four groups.

(i) A northwestern set of 59 earthquakes (NW in Table 1), relocating to a compact area, 145 km in the EW direction by 55 km in the NS one. Depths range from 598 to 683 km, with a slight deepening of the

Table 1
Seismicity of the Vityaz Cluster

Source[a]	Date D/M/Y	Origin time GMT	Epicenter °N	Epicenter °E	Depth (km)	Group[b]	Magnitude [and agency]	Number of stations
TS	18/07/1949	8:27:17.2	−12.690	171.230	572	CE		
TS	5/11/1957	9:54:32.8	−13.010	168.740	646	NW	$6\frac{1}{2}$ MAT	
TS	13/10/1958	5:28:00.8	−14.210	171.640	634	CE		
TS	30/12/1958	16:07:45.0	−14.400	170.560	655	CE		
TS	11/02/1960	4:27:40.8	−14.020	170.120	634	CE		
TS	12/02/1961	12:57:18.8	−13.120	171.220	592	CE		
TS	28/08/1961	7:41:27.8	−12.870	169.430	664	NW	$6\frac{1}{2}$ WEL	
TS	11/05/1962	12:06:42.0	−14.350	170.370	629	CE		020
TS	15/07/1962	8:06:22.8	−14.020	172.420	630	CE		008
TS	3/12/1962	12:50:36.4	−12.920	169.270	631	NW		017
TS	13/01/1963	13:43:42.5	−14.350	171.440	646	CE	4.9 WMO	018
TS	8/02/1963	18:18:07.6	−13.020	170.200	635	NW/CE		013
TS	14/12/1963	5:07:40.2	−13.720	170.030	612	CE	4.4 m_b	007
ISC	14/03/1964	15:05:54.4	−13.820	172.380	613	CE	5.0 m_b	051
ISC	26/06/1964	13:10:29.3	−12.660	169.460	658	NW	4.6 m_b	028
TS	30/06/1964	17:52:35.3	−14.320	173.480	613	CE	4.2 m_b	019
TS	17/09/1964	15:06:13.6	−12.920	169.080	630	NW	4.5 m_b	014
TS	21/01/1965	21:37:27.4	−13.030	169.280	659	NW	4.4 m_b	017
ISC	25/01/1965	1:11:53.6	−14.990	171.390	637	CE	4.3 m_b	013
ISC	30/01/1965	17:42:11.6	−13.050	169.580	644	NW	4.9 m_b	027
ISC	30/01/1965	18:06:20.8	−12.930	169.630	641	NW	5.1 m_b	034
ISC	3/02/1965	18:26:04.9	−14.210	172.810	627	CE		014
ISC	10/04/1965	22:53:04.5	−13.450	170.300	641	CE	5.3 m_b	043
TS	19/04/1965	17:01:10.7	−13.590	170.310	658	CE	3.9 m_b	013
ISC	29/06/1965	2:07:18.2	−13.840	170.620	638	CE	4.6 m_b	017
TS	12/09/1965	19:11:35.0	−14.160	172.830	608	CE	3.9 m_b	009
ISC	13/12/1965	16:50:16.8	−14.280	170.340	642	CE	4.7 m_b	018
TS	7/02/1966	17:00:18.4	−13.360	172.760	620	CE	4.4 m_b	019
ISC	24/04/1966	3:28:50.6	−12.930	169.520	663	NW	4.4 m_b	025
ISC	4/06/1966	8:35:15.3	−14.820	171.170	658	CE	4.7 m_b	028
TS	15/01/1967	6:18:31.8	−13.680	170.850	640	CE	4.6 m_b	013
ISC	14/02/1967	5:02:38.0	−13.360	171.450	629	CE	5.6 m_b	127
ISC	16/03/1967	17:33:07.6	−13.760	170.760	640	CE	4.8 m_b	071
ISC	12/05/1967	1:59:31.7	−13.890	169.970	620	CE	4.5 m_b	038
ISC	25/08/1967	9:09:15.4	−14.350	170.190	634	CE	4.0 m_b	014
ISC	8/01/1968	3:17:12.3	−13.740	171.480	623	CE	5.1 m_b	076
TS	8/01/1968	3:36:50.2	−13.620	171.350	643	CE	3.9 m_b	015
ISC	17/02/1968	19:46:24.8	−13.870	172.940	621	CE	4.3 m_b	030
ISC	4/11/1968	9:07:39.6	−14.200	172.020	578	CE	5.8 m_b	092
ISC	4/11/1968	10:36:22.4	−14.100	172.010	606	CE	4.8 m_b	056
TS	4/11/1968	10:47:12.1	−14.160	172.060	614	CE	4.2 m_b	019
ISC	2/01/1969	15:47:55.4	−12.840	169.090	634	NW	4.7 m_b	035
ISC	30/05/1969	15:38:55.0	−12.620	168.920	647	NW	4.2 m_b	019
ISC	15/10/1969	6:58:21.0	−12.920	169.320	658	NW	4.3 m_b	016
ISC	12/01/1970	10:34:37.1	−12.710	169.240	659	NW	4.2 m_b	017
TS	15/01/1970	6:01:32.6	−13.640	167.140	634	WE	4.4 m_b	014
ISC	1/03/1970	5:22:27.9	−12.970	168.770	625	NW	4.8 m_b	037
TS	2/03/1970	8:29:15.9	−14.580	169.990	607	CE	4.6 m_b	023
ISC	13/12/1970	0:38:05.2	−14.060	170.950	640	CE	4.2 m_b	025
ISC	15/02/1971	7:04:28.4	−14.610	170.460	637	CE	4.3 m_b	020
TS	21/05/1971	10:11:53.2	−14.360	169.920	597	CE	4.0 m_b	019

Table 1 (continued)

Source[a]	Date D/M/Y	Origin time GMT	Epicenter °N	Epicenter °E	Depth (km)	Group[b]	Magnitude [and agency]	Number of stations
ISC	17/09/1971	12:01:18.8	−13.840	170.900	640	CE	4.5 m_b	026
ISC	17/11/1971	10:56:48.2	−12.910	168.430	630	NW	5.1 m_b	025
ISC	22/04/1972	13:18:20.5	−12.860	169.300	655	NW	4.8 m_b	034
ERL	27/02/1973	21:44:46.4	−14.300	170.980	641	CE	4.0 m_b	024
ISC	7/07/1973	0:09:15.1	−15.180	175.060	613	EA	4.8 m_b	024
ISC	25/09/1973	3:38:02.4	−14.770	171.450	623	CE	5.1 m_b	064
TS	4/05/1974	6:36:52.6	−12.690	168.710	643	NW	4.3 m_b	13
ISC	4/05/1974	12:47:28.1	−13.920	172.650	588	CE	5.4 m_b	86
TS	4/05/1974	14:55:36.6	−14.150	173.120	595	CE		13
ISC	5/05/1974	11:28:28.5	−14.120	172.750	602	CE	4.7 m_b	37
ISC	24/08/1974	14:01:53.0	−14.700	170.750	630	CE	4.8 m_b	43
ISC	31/08/1974	1:43:27.4	−12.740	168.700	630	NW	5.0 m_b	20
ISC	20/09/1974	9:58:59.8	−12.730	169.220	650	NW	4.2 m_b	29
TS	22/04/1975	14:26:46.4	−13.000	169.170	646	NW	4.7 m_b	27
ISC	21/11/1975	21:41:30.5	−12.840	168.760	631	NW	4.9 m_b	12
ISC	8/04/1976	1:41:20.2	−14.780	171.880	624	CE	4.7 m_b	13
ISC	16/04/1976	15:55:25.3	−14.460	172.030	620	CE	5.1 m_b	59
ISC	8/05/1976	18:14:02.6	−14.880	172.290	612	CE	4.1 m_b	14
ISC	19/05/1976	19:07:17.6	−12.780	169.210	652	NW	5.1 m_b	92
ISC	19/05/1976	19:10:30.6	−12.700	169.230	642	NW	5.0 m_b	50
ISC	20/05/1976	22:09:00.8	−12.680	169.700	661	NW	4.3 m_b	18
TS	9/06/1976	5:23:44.1	−12.680	167.970	557	WE	4.6 m_b	12
TS	20/07/1976	6:21:51.8	−13.980	170.520	642	CE	4.5 m_b	21
TS	27/08/1976	20:37:19.2	−14.830	175.330	621	EA	4.8 m_b	11
ISC	28/08/1976	10:06:33.9	−14.890	175.320	621	EA	4.9 m_b	51
TS	28/08/1976	13:31:48.7	−14.930	175.370	589	EA	4.6 m_b	15
TS	29/12/1976	8:04:35.1	−13.000	169.000	631	NW	4.2 m_b	14
ISC	17/03/1977	8:50:28.6	−12.980	169.320	657	NW	5.0 m_b	19
TS	17/03/1977	9:17:06.8	−13.030	169.270	661	NW	4.9 m_b	14
TS	17/03/1977	9:18:40.3	−12.900	169.330	660	NW	4.8 m_b	8
ISC	17/03/1977	12:42:31.6	−12.980	169.260	662	NW	5.0 m_b	28
ISC	10/05/1977	18:11:07.8	−14.000	172.130	635	CE	4.4 m_b	22
TS	19/05/1978	7:44:44.9	−12.940	169.030	630	NW	4.2 m_b	22
TS	28/02/1979	1:11:25.2	−13.750	170.120	632	CE		7
ISC	5/06/1979	18:14:19.5	−14.680	171.750	636	CE	5.0 m_b	62
PDE	30/06/1979	22:52:15.7	−12.760	169.170	653	NW	4.9 m_b	86
TS	12/08/1979	17:33:53.0	−12.690	169.500	674	NW	4.2 m_b	18
ISC	15/10/1979	15:23:50.0	−13.030	169.150	636	NW	4.9 m_b	43
ISC	14/12/1979	10:09:43.3	−12.650	169.860	664	NW	4.6 m_b	27
ISC	30/03/1980	21:30:51.4	−14.010	171.860	624	CE	4.1 m_b	29
ISC	21/07/1980	22:47:42.2	−12.900	168.730	626	NW	5.4 m_b	130
ISC	27/11/1980	13:07:17.1	−12.890	169.380	649	NW	4.7 m_b	40
ISC	23/01/1981	16:14:00.7	−12.920	169.370	660	NW	4.4 m_b	31
ISC	25/10/1981	22:50:11.9	−13.980	171.720	645	CE	4.4 m_b	30
ISC	31/10/1981	7:37:19.6	−12.890	169.220	650	NW	5.1 m_b	84
ISC	31/10/1981	12:00:35.4	−12.860	169.200	652	NW	4.5 m_b	43
ISC	3/11/1981	17:35:30.4	−12.950	169.210	660	NW	4.8 m_b	75
ISC	11/03/1983	11:24:57.5	−14.300	172.280	626	CE	4.7 m_b	24
ISC	12/06/1983	9:14:12.6	−12.930	169.010	619	NW	5.3 m_b	138
ISC	26/06/1984	15:27:54.6	−12.800	169.180	656	NW	5.0 m_b	75
ISC	9/07/1984	18:28:07.7	−12.840	169.440	670	NW	4.7 m_b	62
TS	8/09/1984	11:43:24.4	−14.270	169.800	681	CE	4.1 m_b	9

Table 1 (continued)

Source[a]	Date D/M/Y	Origin time GMT	Epicenter °N	Epicenter °E	Depth (km)	Group[b]	Magnitude [and agency]	Number of stations
ISC	15/09/1984	19:59:33.6	−14.100	170.560	651	CE	4.5 m_b	30
TS	13/11/1984	8:10:24.8	−14.560	170.980	670	CE	4.0 m_b	11
ISC	1/12/1984	14:13:34.6	−12.870	169.820	679	NW	4.8 m_b	49
ISC	1/12/1984	14:18:49.1	−12.870	169.790	675	NW	5.1 m_b	59
ISC	22/12/1984	6:09:43.7	−14.160	170.470	651	CE	4.7 m_b	44
ISC	13/01/1985	13:03:46.1	−14.910	171.500	636	CE	4.3 m_b	24
TS	23/01/1985	23:36:05.0	−14.580	170.020	661	CE	4.6 m_b	8
ISC	13/02/1985	11:10:36.1	−12.980	168.840	633	NW	4.8 m_b	101
ISC	3/04/1985	5:35:04.2	−13.850	171.110	645	CE	4.7 m_b	47
ISC	31/08/1985	18:47:28.3	−13.020	169.240	658	NW	4.6 m_b	65
ISC	1/09/1985	21:14:11.4	−14.900	175.100	613	EA	4.3 m_b	11
ISC	24/01/1986	0:59:12.4	−15.020	170.670	660	CE	5.2 m_b	111
ISC	22/08/1986	6:54:55.5	−14.600	174.800	646	EA	4.9 m_b	24
ISC	7/09/1986	1:44:19.9	−12.800	169.520	664	NW	4.9 m_b	119
ISC	8/09/1986	0:36:17.3	−12.850	169.450	662	NW	4.8 m_b	87
ISC	24/09/1986	14:19:37.9	−13.680	173.060	617	CE	5.4 m_b	171
ISC	25/09/1986	0:55:40.3	−14.890	171.520	633	CE	5.2 m_b	108
TS	22/11/1986	8:04:45.0	−14.690	169.880	636	CE	3.8 m_b	10
ISC	6/08/1987	9:52:10.1	−12.960	169.380	660	NW	4.9 m_b	115
ISC	6/08/1987	11:25:59.2	−12.900	169.470	655	NW	5.1 m_b	98
ISC	6/08/1987	11:39:26.0	−13.000	169.400	683	NW	4.8 m_b	24
ISC	11/11/1987	3:16:12.0	−14.270	172.550	590	CE	4.8 m_b	28
ISC	5/02/1988	18:15:26.6	−15.280	175.210	623	EA	4.8 m_b	47
ISC	11/12/1988	12:05:21.0	−14.000	170.500	666	CE	4.2 m_b	64
ISC	15/04/1989	23:48:38.2	−13.880	171.980	630	CE	5.3 m_b	173
TS	4/08/1989	6:22:10.8	−14.670	171.270	638	CE	4.5 m_b	18
TS	24/01/1990	16:19:21.1	−12.830	169.870	683	NW	4.6 m_b	69
ISC	7/02/1991	23:09:05.0	−13.100	168.530	659	NW	4.8 m_b	78
ISC	22/06/1991	8:00:12.7	−14.230	171.660	634	CE	5.0 m_b	103
ISC	1/04/1992	21:02:38.8	−14.690	171.380	634	CE	5.0 m_b	259
ISC	14/12/1992	7:41:01.1	−14.050	170.750	632	CE	5.5 m_b	480
TS	19/01/1993	18:51:29.2	−14.570	170.470	621	CE	4.7 m_b	27
TS	24/12/1993	2:33:27.6	−14.070	170.490	640	CE	4.8 m_b	155
ISC	2/02/1994	2:54:21.1	−14.060	171.270	636	CE	4.9 m_b	353
ISC	2/02/1994	22:15:52.	−14.000	172.500	657	CE	4.1 m_b	30
ISC	4/02/1994	14:57:02.	−14.400	172.000	656	CE	4.4 m_b	16
ISC	12/03/1994	1:49:03.4	−14.530	171.090	624	CE	5.2 m_b	504
PDE	12/03/1994	2:23:23.	−14.600	171.200	659	CE	4.6 m_b	62
TS	3/05/1994	6:53:07.6	−14.260	170.110	639	CE	5.0 m_b	22
ISC	22/05/1994	23:13:02.	−14.600	170.000	630	CE	4.9 m_b	28
TS	5/09/1994	23:52:16.3	−14.660	172.020	618	CE	5.1 m_b	12
ISC	15/11/1994	11:06:39.9	−14.070	171.240	655	CE	4.9 m_b	176
ISC	13/04/1995	2:34:36.6	−13.520	170.490	623	CE	5.6 m_b	621
ISC	13/04/1995	2:47:29.0	−13.700	170.500	669	CE	4.6 m_b	82
ISC	13/04/1995	2:59:13.2	−13.550	170.660	641	CE	4.6 m_b	207
ISC	18/04/1995	18:57:09.8	−13.500	170.550	661	CE	4.5 m_b	110
ISC	15/05/1995	19:57:51.	−14.400	170.600	655	CE	4.1 m_b	22
ISC	20/05/1995	9:48:34.	−13.590	170.610	655	CE	4.5 m_b	126
ISC	7/06/1995	11:02:44.	−13.400	170.480	654	CE	4.6 m_b	2
ISC	7/06/1995	19:57:59.	−13.030	168.730	598	NW	4.7 m_b	187
PDE	16/07/1995	10:59:56.0	−14.065	172.240	550	CE	4.1 m_b	13
PDE	30/09/1995	15:14:33.7	−13.172	169.884	653	NW/CE	4.0 m_b	11

Table 1 (continued)

Source[a]	Date D/M/Y	Origin time GMT	Epicenter °N	Epicenter °E	Depth (km)	Group[b]	Magnitude [and agency]	Number of stations
PDE	4/01/1996	23:19:57.1	−12.730	169.212	655	NW	4.0 m_b	32
PDE	10/01/1996	04:09:45.1	−12.548	169.215	600	NW	4.6 m_b	13
PDE	28/03/1996	14:05:49.9	−13.860	170.753	578	CE	4.1 m_b	35
PDE	5/04/1996	17:07:39.1	−14.280	170.405	605	CE	4.3 m_b	33
PDE	23/05/1996	19:25:46.9	−13.841	171.751	598	CE	4.4 m_b	104
PDE	3/06/1996	12:57:34.0	−12.661	169.305	600	NW	4.0 m_b	16
PDE	13/06/1996	08:50:53.3	−12.780	169.066	600	NW	4.2 m_b	19
PDE	14/06/1996	23:24:13.0	−14.835	171.856	500	CE	4.2 m_b	13
Event at intermediate depth								
TS	16/05/1983	06:10:19.0	−12.840	169.14	160	ID	3.8 m_b	8

[a]Key to source of retained hypocenter: TS, Relocated in this study; ISC: Location by International Seismological Centre retained; PDE: Location by Preliminary Determination of Epicenters retained (mostly recent events with ISC data not yet available); ERL: Location from Environmental Research Laboratories retained; HRV: Harvard Centroid moment tensor location retained.
[b]Subgroup identification: NW: Northwestern group (56 events); CE: Central group (88 events); EA: Eastern group (7 events); WE: Isolated events (2) at Western end of NW; NW/CE: Transition events (2) between NW and CE; ID: Intermediate-depth above Vityaz Cluster. See Appendix A for details.

seismicity to the east. Magnitudes reach $m_b = 5.4$; two historical events in 1957 and 1961 are given magnitudes (of unspecified type) of $6\frac{1}{4}$ and $6\frac{1}{2}$. Most of the activity in the NW group took place during the 1970s and 1980s.

(ii) A pair of isolated events occurs west of this group (WE in Table 1): 09 Jun 1976, 12.68°S; 167.97°E, 557 km, $m_b = 4.6$; and 15 Jan 1970, 13.64°S; 167.14°E, 634 km, $m_b = 4.4$. Because of this apparent isolation, we gave them special scrutiny.

- *09 Jun 1976:* The quality of the location is excellent (18 stations with $\sigma = 1.05$ s). Bootstrap deletion of stations could not move the earthquake significantly, and the Monte Carlo ellipse was 40 km (NS) by 15 km (EW), with depths of 541 to 571 km.
- *15 Jan 1970:* The quality of the location is also excellent (17 stations with $\sigma = 1.26$ s). No bootstrap deletion of stations could move the earthquake significantly, and the horizontal Monte Carlo ellipse was circular ($r = 15$ km), with depths of 615 to 645 km.

We conclude that both relocated hypocenters (labeled with Julian dates 70015 and 76161 on Fig. 5) are doubtless isolated from the rest of the Vityaz population. The distance between the two events is comparable to the transverse dimension of the whole Vityaz cluster along a SSW–NNE direction. This suggests that the pair is part of the Vityaz seismic structure, and not related to the Vanuatu WBZ. Furthermore, their location (especially for the second event), *directly underneath* the Vanuatu WBZ, and west of its deepest part ($h = 300$ km in the north; see Fig. 6), argues that they are not part of the Vanuatu slab, or its continuation.

(iii) The remainder of the Vityaz cluster consists mainly of a central group of 93 somewhat scattered hypocenters extending about 335 km in longitude, by 225 km in latitude (CE in Table 1). Depths range from 572 to 681 km, although the events located deepest and shallowest are generally small or historical earthquakes, for which depth control, as indicated by the Monte Carlo results, is poor. A tighter depth range, controlled by robust ISC locations, would be 580 to 660 km. Magnitudes in the central group reach $m_b = 5.8$. The central group was active principally during the 1960s, 1970s and 1990s.

(iv) Finally, a small, eastern group of 7 earthquakes (EA in Table 1) clusters near 15°S, 175°W. Its dimensions (~ 30 by 30 km) are comparable to the size of the Monte Carlo ellipses of these small events (all have $m_b < 5$).

These groups are easily identified on the map, but a few shocks did occur between them: two events (NW/CE in Table 1) took place between the northwestern and central groups. One is a small shock (no magnitude given) on 08 Feb 1963. Its Monte Carlo ellipse covers the gap between the groups, and it

Table 2
Deep earthquakes of the Southern Fiji Basin

Source	Date D/M/Y	Origin time GMT	Epicenter °N	Epicenter °E	Depth (km)	Magnitude m_b	Number of stations
North Finger							
ISC	28/01/1966	4:36:45.3	−17.64	177.01	556	5.5	054
ISS	30/12/1966	1:00:24.4	−18.06	179.16	650	5.1	067
ISS	30/12/1966	13:14:48.3	−18.09	179.20	639	4.2	019
TS	24/11/1971	13:46:59.0	−17.65	177.78	544	4.0	009
ISC	26/04/1972	1:33:18.9	−18.23	173.01	591	5.1	069
ISS	19/12/1974	10:59:00.1	−17.60	179.32	637	4.5	25
TS	18/05/1978	15:51:28.8	−17.51	178.60	619	3.6	18
ISS	28/03/1983	21:41:56.3	−17.75	178.77	560	4.5	22
ISC	23/11/1983	15:18:23.8	−17.73	178.90	569	4.6	13
ISC	27/03/1984	1:37:58.2	−17.71	179.80	621	4.8	36
ISC	30/11/1986	9:18:43.6	−17.78	179.51	601	4.8	80
ISC	26/11/1992	19:49:23.3	−18.36	178.56	661	5.2	171
PDE	25/02/1996	23:15:30.7	−17.94	179.45	662	4.7	36
PDE	11/03/1996	14:38:11.7	−17.55	179.24	600	4.3	14
South Finger							
ISC	25/10/1968	10:13:30.0	−19.97	179.72	505	4.2	015
ISC	18/11/1970	16:43:14.8	−21.81	175.23	572	5.6	081
ISC	5/01/1973	21:29:09.7	−21.35	175.38	591	5.2	056
ISC	13/04/1973	19:54:14.0	−19.92	179.88	658	5.0	043
ISC	15/12/1973	10:54:52.2	−21.59	175.17	569	5.3	078
ISC	24/03/1974	0:12:45.2	−21.17	175.78	595	4.6	39
ISC	10/11/1976	14:50:04.8	−19.61	179.77	536	4.9	37
ISC	18/01/1977	14:35:33.5	−21.37	175.00	542	4.6	30
ISC	22/04/1980	10:54:02.0	−19.70	179.40	510	4.4	8
ISC	30/04/1980	11:25:33.3	−20.26	178.79	518	5.0	22
ISC	27/07/1980	0:28:32.1	−19.64	179.92	524	5.3	105
TS	18/08/1980	11:22:13.0	−19.88	179.72	466	5.0	18
ISC	26/05/1986	19:06:16.4	−20.15	178.85	543	6.4	508
ISC	26/05/1986	19:48:37.2	−20.64	177.79	633	5.5	159
ISC	28/05/1986	7:31:26.0	−20.00	178.80	565	4.8	16
TS	29/05/1986	22:58:04.9	−20.19	178.88	541	4.9	44
TS	30/05/1986	2:13:30.1	−20.04	178.48	613	4.1	
ISC	3/06/1986	9:41:44.8	−20.00	178.80	547	4.7	41
ISC	5/06/1986	0:17:48.8	−20.24	178.90	538	5.2	92
ISC	9/06/1986	0:48:19.1	−20.18	178.88	547	4.9	54
ISC	4/10/1990	17:33:02.0	−20.00	180.00	602	5.3	9
TS	26/10/1993	21:48:33.5	−20.15	179.96	547	4.1	10
Other deep events under the South Fiji Basin							
ISC	1/10/1965	13:22:28.4	−19.89	174.46	541	6.2	073
ISC	2/06/1990	3:25:33.0	−20.70	173.10	502	3.9	20
Other deep events in the box on Fig. 2							
TS	1/08/1964	2:27:21.9	−20.12	−179.17	630	4.4	008
TS	9/11/1964	23:35:45.6	−18.06	−178.35	562	3.8	005
ISC	9/01/1969	11:48:50.2	−18.95	179.52	662	4.5	018
TS	14/04/1980	13:36:29.0	−18.62	179.74	676	4.5	12
TS	16/10/1984	0:08:03.7	−17.88	−179.54	606	4.3	15
TS	26/06/1988	6:02:43.5	−20.23	−178.48	688	4.5	14

Table 2 (continued)

Source	Date D/M/Y	Origin time GMT	Epicenter °N	Epicenter °E	Depth (km)	Magnitude m_b	Number of stations
Other deep events in the box on Fig. 2 (continued)							
TS	28/01/1990	1:25:23.7	−19.09	−179.94	642	4.4	12
TS	27/03/1993	0:58:46.8	−20.84	179.55	620	4.6	13
TS	11/06/1993	7:49:09.4	−18.87	179.32	536	4.6	9

could belong to either, as it could also be genuinely in between. The second event is a small ($m_b = 4.0$) earthquake on 30 Sep 1995; in the absence of ISC data, its location is imprecise.

Finally, we note that the shallowest events in the Vityaz cluster tend to be near its northern edge; if this trend is real and expresses a systematic dip of the cluster, the latter would be in the SSW direction.

3.2. Seismicity above the Vityaz cluster

In order to explore the possibility of a seismically continuous slab above the Vityaz cluster, all the seismicity of the North Fiji Basin was re-examined, even earthquakes originally listed as shallow. As part of this effort, we identified as belonging to the deep Vityaz cluster the events of 18 July 1949, 13 Oct 1958 and 30 Dec 1958, all listed as surficial ($h = 0$), but relocated at 572, 634 and 655 km, respectively. Table 4 lists confirmed or relocated shallow epicenters ($h \leq 50$ km) in the North Fiji Basin.

Diffuse seismicity at shallow depths has long been documented in the North Fiji Basin (e.g., Hamburger and Everingham, 1986; Hamburger and Isacks, 1987). The NEIC lists 18 events with $50 \leq h \leq 500$ km under the North Fiji Basin. Of those, the deepest two (given with $h = 450$ and 500 km respectively) relocate deeper into the Vityaz cluster. Another six relocate at intermediate depth inside the Vanuatu WBZ to the west. Nine more earthquakes relocate to shallow depths ($h \leq 50$ km); this includes four for which the dataset has no depth resolution, and is fit just as well by a shallow source.

This leaves the case of a single earthquake relocating at intermediate depth above the Vityaz cluster (16 May 1983; 09:10 GMT; 12.84°S, 169.14°E; $h =$ 160 km; $m_b = 3.7$). Despite the small magnitude of the event, and the sparse available dataset (8 P times, mostly at regional distances), the solution for this event appears robust. If this earthquake did actually occur as an isolated shock at 160 ± 10 km depth, (above the Northwestern group of deep Vityaz earthquakes, and about 220 km away from the nearby Vanuatu WBZ), it would suggest that seismogenic material does exist directly above the Northwestern group of the Vityaz cluster. The final geometry of the Vityaz cluster and its associated intermediate depth event is presented in cross-section on Fig. 6 (in a direction perpendicular to the Vanuatu arc) and Fig. 7 (in a direction perpendicular to the Vityaz Trench). The tentative nature of the location of the 1983 event is underscored by a question mark on these figures. Because of the possible importance of this result, we detail various aspects of this event's relocation in Appendix A.

3.3. The outboard seismicity of the South Fiji Basin

3.3.1. Deep structure of the Tonga Wadati–Benioff Zone

Before discussing our findings on the deep earthquakes outboard of the Tonga WBZ, it is worthwhile to review its deep structure in order to define what is outboard and what is not, and to identify possible ongoing processes leading to outboard events.

The bottom of the Tonga WBZ displays an extremely complex morphology that evidently reflects its intense interaction with the lower mantle (Giardini and Woodhouse, 1984, 1986) and the deformation connected with the eastward migration of the Tonga trench (Van der Hilst, 1995). The deepest part of the zone of semi-continuous Tonga WBZ typically shows an abrupt buckling and westward deflection of hypocenters and hence a reduction of apparent dip (e.g., Fig. 8). To the west is a band of shocks, discontinuous in the north, that is offset from the main WBZ (See Figs. 2 and 8 of this paper, and also

Table 3
Other deep seismicity of the Southern Fiji Basin

Source	Date D/M/Y	Origin time GMT	Original location			Relocation			Magnitude [and agency]	Number of stations
			Lat. (°N)	Long. (°E)	Depth (km)	Lat. (°N)	Long. (°E)	Depth (km)		
Events initially in box but relocating to the Vanuatu WBZ (†: Monte-Carlo ellipsoid intersects WBZ)										
TS	09/09/1920	18:56:26	-15	171.5	0	-12.88	165.78	10		9
TS	03/05/1930	12:23:40.7	-13	170	0	-13.51	166.17	10		8
TS	14/07/1933	1:38:45.0	-20.5	170	445	-19.45	168.83	276		14
TS	03/06/1934	16:15:55.3	-15.2	168.8	0	-15.29	167.40	251		13
TS	09/04/1938	09:10:31.9	-15.0	168.5	0	-15.24	167.98	10		18
TS	18/12/1939	06:26:21.0	-15	168.5	0	-15.26	168.26	10		16
TS	21/07/1950	20:32:12.5	-16.1	168.3	0	-16.24	168.53	106.	6.87 PAS	40
TS	23/09/1955	12:23:43.3	-15	170	0	-17.29	167.03	10		8
TS	12/10/1956	18:40:39.8	-17.25	170.0	200	-18.22	170.06	224†		011
TS	19/06/1958	11:11:33.9	-15.5	168.5	0	-15.16	167.39	139		15
TS	27/01/1959	02:20:18.7	-15.0	168.5	0	-14.99	166.51	10		9
TS	29/09/1962	20:42:29.4	-14.2	168.2	198	-14.63	167.52	166		10
TS	22/03/1963	11:56:46.1	-15.3	168.2	33	-15.49	167.82	10		6
TS	02/11/1964	8:10:13.5	-16.9	169.7	255	-16.98	168.67	235	4.7 m_b	013
TS	08/12/1961	14:27:13.4	-15.0	168.5	178	-15.72	168.1	164		008
ISC	29/11/1964	6:20:03.4	-19.4	169.2	324	-19.18	169.33	254	4.9 m_b	018
TS	12/09/1965	6:04:23.9	-18.2	169.2	313	-18.99	169.66	256	4.2 m_b	009
TS	06/07/1966	12:11:58.1	-19.6	172.0	293	-19.18	170.00	311	4.5 m_b	007
TS	22/07/1966	02:44:22.3	-13.9	170.4	104	-14.62	167.62	151		006
TS	17/02/1967	17:34:56	-13.736	168.520	155	-14.47	168.24	131	4.6 m_b	6
ISC	19/04/1973	11:26:36.2	-18.341	169.434	301	-18.28	169.53	299	4.7 m_b	050
TS	11/01/1973	12:34:14.6	-13.9	168.9	44	-15.12	167.09	90	4.5 m_b	14
TS	27/11/1973	18:40:34.5	-20.978	170.444	202	-20.98	170.49	198†		007
TS	28/09/1974	02:43:41.1	-20.3	168.8	223	-20.77	170.37	184†	4.1 m_b	6
TS	15/04/1984	10:16:03.5	-15.500	168.738	255	-15.94	168.42	274	4.6 m_b	22
TS	28/02/1986	15:08:24.3	-14.5	168.4	33	-15.07	167.01	157		8
TS	19/07/1986	23:38:13.4	-15.1	168.5	109	-16.20	167.94	177	4.7 m_b	18
Events initially in box but relocating to the Tonga WBZ (†: Monte-Carlo ellipsoid intersects WBZ)										
TS	15/03/1920	12:05:30	-20.	176.5	223	-22.64	-179.19	690		
TS	21/09/1951	3:21:07.3	-18.70	175.44	150	-20.86	-178.20	299		019
TS	22/12/1953	04:33:45.0	-22.	177.	180	-21.76	179.95	650		
ISC	25/07/1972	4:08:32.0	-14.883	179.446	508	-25.00	179.64	517	3.6 m_b	009
ISC	23/09/1979	2:26:38.4	-23.633	176.939	398	-23.58	179.26	545	4.3 m_b	13
TS	22/10/1983	17:57:00.5	-17.662	179.512	528	-20.70	-177.76	508	4.5 m_b	6
TS	20/04/1993	16:48:01.5	-14.205	-179.261	505	-14.21	-179.22	497†	4.3 m_b	20
ISC	29/08/1994	14:16:05.1	-21.22	179.26	674	-21.8	-179.2	628	4.4 m_b	23
Events in box initially deeper than 50 km, but relocating shallower than 50 km										
TS	1/12/1933	10:26:40.6	-20.5	169	140	-20.25	168.55	10		12
TS	22/09/1941	17:08:16	-22.0	175	60	-22.07	174.88	13	6.5 PAS	
TS	13/05/1959	1:00:51.8	-17.15	174.12	63	-17.05	174.26	7		13
ISC	04/05/1960	18:29:51.2	-20.51	172.76	77	-20.33	173.01	0	5.63 MAT	
TS	10/06/1960	11:31:39.3	-16.32	172.7	56	-16.40	172.65	10		
ISS	20/07/1960	20 59 12.0	-20.5	169.0	200	-19.93	169.99	29		130
TS	21/07/1960	00:10:47.7	-20.5	169	200	-20.04	170.10	15		9
TS	17/05/1961	00:55:18.9	-14.4	170.4	137	-13.87	170.10	10		
ISS	22/10/1961	09:50:23	-20.0	172.7	65	-19.85	172.87	0	5.5 BRK	
TS	30/12/1961	15:31:36.1	-16.0	170.0	65	-15.82	169.70	10		010

Table 3 (continued)

Source	Date D/M/Y	Origin time GMT	Original location			Relocation			Magnitude [and agency]	Number of stations
			Lat. (°N)	Long. (°E)	Depth (km)	Lat. (°N)	Long. (°E)	Depth (km)		
Events in box initially deeper than 50 km, but relocating shallower than 50 km (continued)										
TS	11/03/1962	07:18:44.9	-13.9	172.1	133	-14.08	172.43	10		24
TS	06/03/1964	20:42:55.8	-19.5	174.5	56	-19.40	174.63	29	4.6 m_b	14
TS	31/05/1964	17:15:26.8	-13.6	172.1	73	-13.61	172.31	23	5.3 m_b	62
ISC	22/02/1965	21:38:15.5	-16.8	175.7	73	-16.84	176.01	39	4.9 m_b	39
ISC	21/02/1966	17:17:13.2	-18.0	167.7	470	-17.89	167.67	34		015
ISC	31/07/1966	11:49:27	-19.6	173.7	84	-19.78	173.59	32	4.9 m_b	37
TS	17/05/1967	16:13:29.2	-16.6	175.5	80	-16.62	175.94	10	4.9 m_b	31
TS	27/07/1968	10:51:32.1	-19.2	175.7	88	-19.15	175.90	23	5.4 m_b	65
TS	02/11/1968	03:18:42.1	-16.6	175.9	114	-16.56	176.08	10	4.9 m_b	36
ISC	16/11/1968	07:45:48.6	-16.6	175.9	66	-16.58	175.98	36	5.7 m_b	103
ISC	31/10/1969	07:27:54.7	-17.3	174.2	56	-17.25	174.3	42	5.1 m_b	83
ISC	31/10/1971	04:52:48	-18.0	177.4	72	-18.18	177.1	16		15
ISC	01/11/1971	09:59:43.5	-10.3	169.7	54	-10.31	169.77	46	5.3 m_b	57
ISC	10/12/1971	08:32:15	-21.1	173.6	50	-20.87	173.6	35	4.9 m_b	21
ISC	01/01/1972	22:05:54	-16.7	174.8	56	-16.85	174.90	11	5.8 m_b	138
TS	13/02/1972	13:01:44.4	-19.2	175.1	73	-19.27	175.48	10	4.8 m_b	62
TS	14/10/1972	14:51:14.8	-14.3	172.9	60	-14.16	173.09	10	5.3 m_b	67
ISC	14/05/1973	17:11:12.8	-16.6	175.9	54	-16.63	175.86	45	5.7 m_b	135
ISC	03/03/1974	18:07:50	-16.7	176.8	90	-16.89	176.99	39	5.0 m_b	40
ISC	02/06/1975	19:32:53	-20.8	173.1	56	-20.78	173.24	19	5.3 m_b	86
TS	11/09/1975	03:35:16.6	-20.3	174.4	63	-20.21	174.68	16	4.7 m_b	36
TS	12/02/1976	06:47:58.9	-16.8	174.9	93	-17.3	175.5	29	4.5 m_b	15
ISC	18/05/1976	04:54:50.7	-21.6	173.3	52	-21.58	173.43	36	5.4 m_b	79
TS	22/02/1979	22:28:40.2	-21.0	174.3	51	-21.01	173.98	8	4.5 m_b	20
ISC	15/02/1980	18:51:32	-20.2	173.6	59	-19.6	173.61	15	4.6 m_b	20
TS	01/05/1982	05:23:24.8	-17.2	176.7	64	-16.71	176.60	6	4.8 m_b	26
ISC	16/02/1985	14:00:29.4	-18.441	178.035	338	-23.60	-174.86	0	4.3 m_b	11
ISC	06/03/1990	23:28:26	-21.44	175.82	50	-21.5	175.91	12	5.0 m_b	31
TS	03/10/1991	06:31:48.3	-20.08	177.97	110	-11.44	177.72	10	4.4 m_b	7
TS	03/12/1991	02:53:50.6	-13.27	175.80	130	-12.98	175.81	10	4.3 m_b	8
Events initially in box ($h \geq 50$ km), but for which dataset has no depth control (Shallow solution acceptable)										
TS	03/06/1926	4:46:56	-15.	168.5	60	-15.0	168.2		7.10 PAS	
TS	16/02/1936	14:16:51.0	-24	173	160	-23.58	173.18	10		13
TS	14/07/1938	23:31:31	-22.	175	60	-15.0	168.2		6.00 PAS	
TS	21/07/1940	5:16:03.0	-16.	169.5	160	-17.8	170.2		6.00 PAS	
TS	08/09/1960	12:32:57.6	-18.5	177.6	79	-18.4	177.6	10		4
TS	01/02/1961	06:27:18.9	-13.6	173.4	50	-13.51	173.66	10		
TS	16/03/1962	15:25:41.1	-21.8	173.3	83	-21.97	173.63	10		24
CGS	12/10/1963	0:38:12.5	-18.60	179.80	347	-20.39	-179.21	10	4.3 m_b	6
TS	31/05/1964	18:34:15.5	-13.3	171.8	111	-13.42	172.49	10	4.7 m_b	13
TS	26/04/1967	21:46:30.5	-16.5	175.6	116	-16.42	176.00	20	4.8 m_b	47
TS	31/10/1969	07:34:10.0	-17.3	174.3	57	-17.11	174.29	10	5.1 m_b	43
TS	30/08/1974	13:40:20.1	-17.0	176.1	85	-16.84	176.49	20	3.9 m_b	16
TS	12/12/1976	23:07:00.2	-21.8	173.0	71	-21.93	173.25	10		11
TS	21/04/1980	22:31:49.7	-16.8	176.4	56	-16.82	176.54	10	4.1 m_b	13
TS	22/11/1984	07:57:47.8	-15.2	171.1	68	-14.62	170.86	10	4.4 m_b	11
TS	24/09/1985	19:44:29.4	-17.0	177.9	64	-16.41	178.16	10	4.8 m_b	28
TS	16/07/1987	23:26:50.0	-16.7	175.1	58	-16.76	174.99	10	4.1 m_b	16

Table 3 (continued)

Source	Date D/M/Y	Origin time GMT	Original location			Relocation			Magnitude [and agency]	Number of stations
			Lat. (°N)	Long. (°E)	Depth (km)	Lat. (°N)	Long. (°E)	Depth (km)		
Events initially in box but which could not be reliably relocated										
TS	18/02/1930	06:07:28	-15.5	171	0					
TS	03/05/1930	15:22:58	-13.0	170	0					
TS	18/11/1939	00:13:32	-15.0	175.0	0					
TS	2/05/1940	8:24:00.0	-19.50	169.50	370					
CGS	13/10/1940	13:25:42.0	-23	171	200				No data	
CGS	04/07/1949	13:47:58.0	-21.	174.	100					
CGS	23/06/1958	07:19:02.0	-15.5	168.5	0					
CGS	8/02/1964	0:29:48.0	-19.00	-180.00	600				4.0 m_b	5
CGS	6/04/1967	21:38:21.2	-22.46	172.74	485				No data	
CGS	10/04/1978	21:48:41.5	-20.437	168.92	227					006
PDE	29/01/1996	15:39:55.8	-13.843	168.643	33				No ISC data yet	15
PDE	8/02/1996	08:46:29.2	-14.056	167.569	33				No ISC data yet	13
PDE	29/04/1996	10:11:21.2	-17.488	170.786	158				No ISC data yet	12

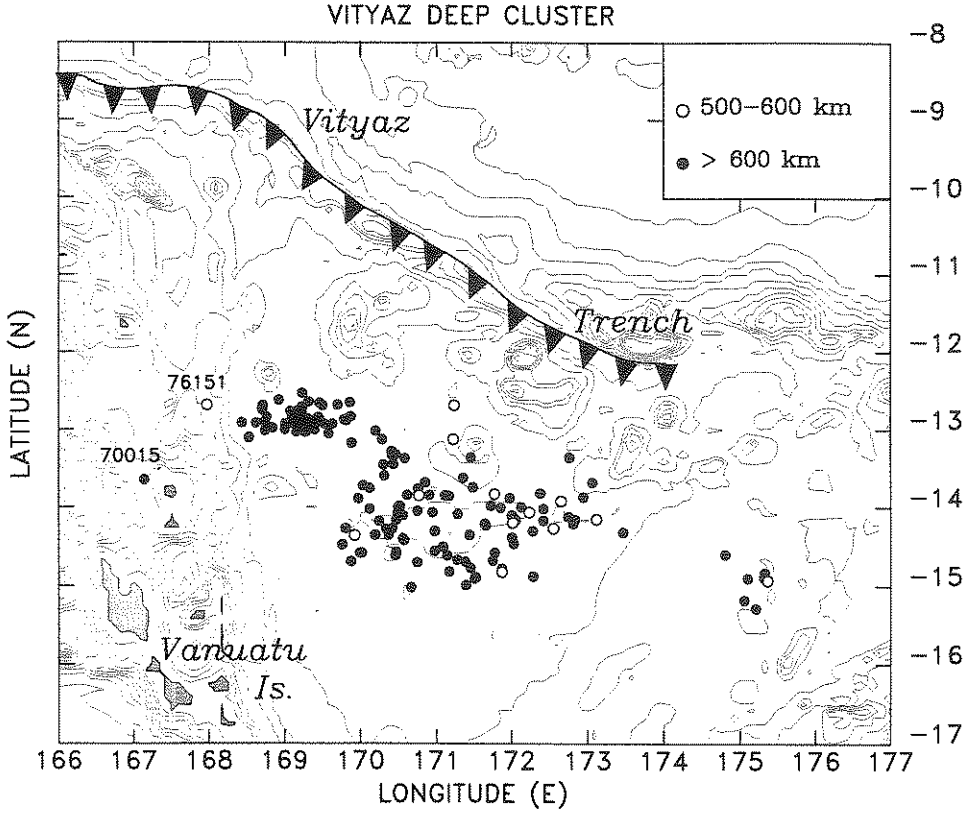

Fig. 5. Epicenters of the Vityaz group of deep earthquakes plotted on a map of the bathymetric contours of the North Fiji Basin and Vityaz Trench at 1000-m intervals. The two westernmost members of the group whose significance is discussed in the text are labeled with the corresponding Julian dates.

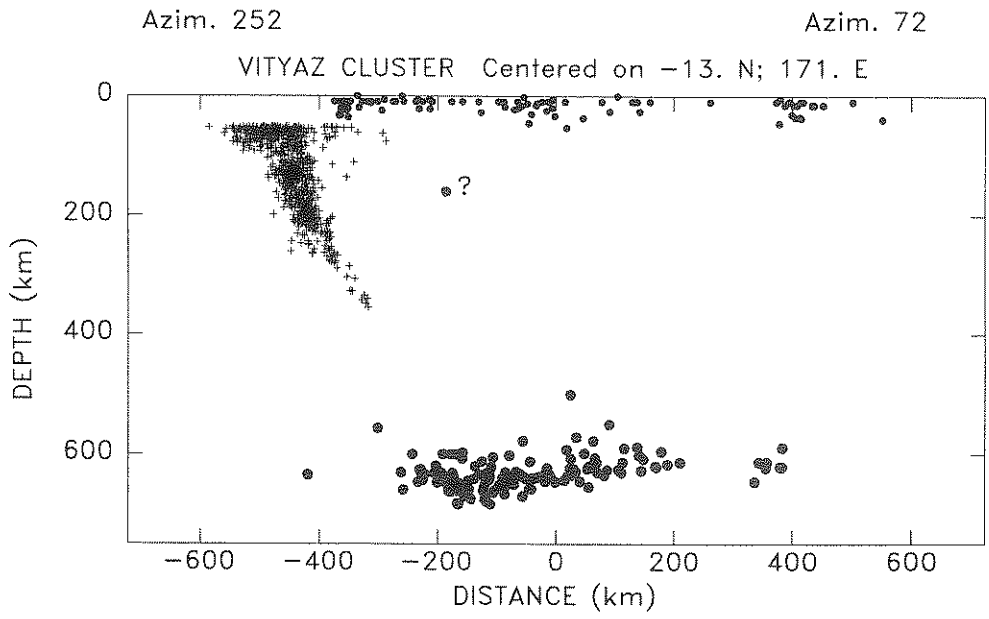

Fig. 6. Cross-section perpendicular to the Vanuatu Trench and including the Vityaz group of deep earthquakes (closed circles). Note the discordance of the geometry of the Vityaz group with the downdip projection of the Vanuatu WBZ (plus symbols). The question mark shows the provisional location of the shock of 16 May 1983, as discussed in Appendix A.

Figs. 1 and 2 in Giardini and Woodhouse (1984) and Figs. 1 and 2 in Lundgren and Giardini (1994)), with shocks as shallow as 550 km and as deep as 680 km, commonly occurring in a steeply inclined segment, especially at latitudes between 22 and 27°S where the band is nearly continuous. A straightforward interpretation of the westward offset of this band is that it represents a fragment of a formerly-continuous slab that was anchored during an earlier attempt to penetrate into the lower mantle, and later sheared off upon trenchward migration of the rest of the slab. Giardini and Woodhouse (1984) document numerous examples of fault-like clusters of earthquakes with CMT mechanisms consistent with the sense of offset of this western band of earthquakes and the main Tonga WBZ. The focal mechanisms of events in the offset band of events are different from those in the main WBZ Lundgren and Giardini (1994), indicating that its material has a different stress state, presumably because it is no longer attached to the main Tonga slab above it. The structure of these earthquakes in the offset band may well be indicative of the processes leading to the occurrence of outboard events to the west.

3.3.2. Deep outboard seismicity west of the bottom of the main Tonga WBZ

We have identified at least 48 deep events that are clearly west of this complex bottom of the main Tonga WBZ. In contrast with the Vityaz cluster, the dataset of deep seismicity west of the Tonga WBZ is much more sparse and scattered. The westernmost events consist of a set of only *eight* earthquakes, spread over approximately 165,000 km^2, between 18 and 22°S; 172 and 176°W, with depths ranging between 540 and 580 km. We retained the ISC locations of all these earthquakes, whose magnitudes ($m_b \geq 5$ in 5 out of the 8 cases) result in precise, robust locations.

To the east of this group, we identify two fingers of seismicity extending westward from the Tonga–Fiji WBZ at respectively 17.6°S; 179.6°E (Northern Finger) and 19.5°S; 179°W (Southern Finger). A half-dozen more shocks are scattered between the two fingers east of 179°E.

What makes this observation remarkable is that the two fingers seem to link up with the scattered seismicity to the west; namely, the Southern Finger extends linearly along an azimuth of N246°E into the

Table 4
Confirmed shallow seismicity of the North Fiji Basin

Source	Date D/M/Y	Origin time GMT	Original location			Relocation			Magnitude [and agency]	Number of stations
			Lat. (°N)	Long. (°E)	Depth (km)	Lat. (°N)	Long. (°E)	Depth (km)		
TS	29/06/1928	22:49:41.4	−15.0	170.5	0	−15.7	170.64	10	7.1 PAS	13
TS	02/05/1930	06:01:39.1	−13	170.0	0	−14.48	168.68	7		14
TS	08/10/1930	10:19:17.9	−13.5	169.0	0	−13.60	168.57	10	6.9 PAS	133
TS	16/10/1930	20:45:55.1	−14.5	175.0	0	−12.91	178.83	10		6
TS	18/03/1936	11:48:28.6	−14.6	168.4	0	−14.82	168.52	10		14
TS	13/11/1949	20:43:18.7	−15.0	168.0	0	−15.12	168.07	10		20
TS	11/01/1952	00:05:45.0	−13.2	174.8	33	−13.83	174.90	10		18
TS	24/06/1952	03:15:50.5	−14.5	168.5	0	−14.45	168.25	20		21
TS	03/03/1958	04:06:18.1	−14.5	168.5	0	−14.69	168.00	10.		19
ISS	31/05/1958	19:32:34	−15.37	168.53	0	−15.37	168.53	0	7.2 PAS	
TS	16/06/1958	07:13:40.1	−15.0	169.0	0	−15.49	168.65	10		16
TS	27/07/1958	17:01:30.0	−15.5	169	0	−15.92	168.60	10		7
TS	01/11/1958	17:25:47.3	−15.5	169	0	−15.57	168.38	10		9
TS	17/02/1959	11:21:17.8	−15.0	168.5	0	−15.28	168.27	10		11
TS	10/03/1960	02:28:59.7	−13.82	169.83	0	−13.64	169.68	10		8
TS	13/07/1960	14:28:49.3	−15	168.5	0	−15.21	168.20	33		15
TS	14/04/1961	12:03:59.1	−14.9	168.2	26	−14.92	168.14	19		13
TS	15/08/1961	17:51:15.7	−14.8	168.3	36	−14.79	168.10	10		19
TS	17/10/1961	09:51:33.2	−14.9	168.4	25	−15.24	168.82	10		11
TS	30/11/1961	14:14:28.3	−14.4	170.9	42	−14.36	170.84	10	5.13 MAT	14
TS	26/02/1962	16:43:24.4	−13.9	172.2	33	−13.91	172.20	26		9
ISS	01/03/1962	23:41:11.5	−14.0	172.1	33	−13.91	172.33	0		
TS	22/01/1963	17:07:05.9	−14.2	168.5	33	−13.93	168.27	10		8
TS	07/03/1963	03:40:43.3	−15.1	168.2	26	−15.06	168.19	10	4.8 m_b	14
TS	11/01/1964	09:24:11.9	−14.1	169.6	33	−14.05	169.64	10	4.9 m_b	9
TS	29/08/1964	12:49:56.5	−13.3	172.4	33	−13.46	172.54	26	4.9 m_b	17
ISC	29/08/1964	13:25:22.3	−13.7	172.6	33	−13.44	172.45	10	5.0 m_b	21
TS	30/08/1964	20:37:06.4	−13.6	172.4	33	−13.47	172.42	10	4.9 m_b	23
TS	30/08/1964	22:30:21.7	−13.7	172.5	33	−13.56	172.52	10		12
ISC	16/09/1965	21:02:40.4	−15.3	168.4	25	−15.29	168.35	21	4.9 m_b	27
TS	02/12/1965	06:44:49.9	−15.1	168.3	36	−14.94	168.21	10	4.4 m_b	12
TS	20/02/1966	10:28:52.0	−15.3	173.1	33	−15.29	173.11	10	4.8 m_b	17
ISC	31/05/1966	19:59:46	−15.2	168.2	21	−15.14	169.19	1	5.0 m_b	22
TS	23/01/1967	03:09:05.7	−13.08	168.36	25	−13.00	168.33	10	4.7 m_b	13
TS	29/09/1967	20:12:58.7	−14.2	168.4	41	−14.09	168.32	12	4.1 m_b	9
ISC	16/11/1967	22:26:21.4	−13.9	171.8	22	−13.77	171.71	37	4.8 m_b	26
ISC	03/10/1971	03:24:38.1	−14.7	171.7	10	−14.60	171.69	10	5.5 m_b	135
TS	13/12/1972	17:14:45.8	−13.32	172.33	33	−13.32	172.41	10	5.0 m_b	12
ISC	20/02/1973	18:10:44.5	−15.2	168.2	32	−15.13	168.15	32	4.9 m_b	29
TS	11/07/1973	18:28:57.9	−13.8	169.0	9	−13.82	169.09	10	4.2 m_b	13
ISC	03/08/1973	15:04:41	−13.8	169.0	33	−13.74	169.17	6	5.3 m_b	51
TS	22/12/1973	14:19:00.8	−14.8	173.7	33	−14.73	173.13	10	5.5 m_b	95
TS	31/12/1973	11:09:23.7	−13.5	175.2	33	−13.36	175.18	10	5.1 m_b	30
ISC	15/12/1974	15:32:03	−15.3	168.2	33	−15.41	168.25	34	4.7 m_b	14
TS	10/01/1975	19:22:07.7	−15.0	168.2	17	−14.94	168.24	36	5.1 m_b	57
TS	09/04/1975	16:02:10.9	−14.8	172.3	33	−14.62	172.30	10	4.8 m_b	13
ISC	22/08/1976	21:09:42	−14.0	170.9	31	−14.03	170.95	31	5.6 m_b	131
TS	29/12/1976	15:29:50.2	−13.6	173.7	33	−13.44	173.68	10	4.6 m_b	16
TS	15/01/1977	21:09:47.0	−14.3	170.5	33	−14.11	170.44	10	5.0 m_b	23
ISC	24/01/1977	10:29:30	−13.5	168.3	21	−13.53	168.32	25	5.3 m_b	82

Table 4 (continued)

Source	Date D/M/Y	Origin time GMT	Original location			Relocation			Magnitude [and agency]	Number of stations
			Lat. (°N)	Long. (°E)	Depth (km)	Lat. (°N)	Long. (°E)	Depth (km)		
TS	07/10/1978	15:11:20.8	−14.1	168.7	41	−13.95	168.67	10		15
TS	09/06/1981	11:33:06.1	−13.4	168.9	33	−13.53	168.88	10	4.7 m_b	20
TS	30/12/1981	19:03:32.2	−14.9	169.1	33	−14.87	169.13	10		13
TS	22/10/1982	12:40:01.4	−13.8	169.2	33	−13.76	169.22	10	4.5 m_b	19
TS	04/04/1983	03:15:32.2	−14.3	171.5	33	−14.35	171.40	7	5.5 m_b	42
ISC	23/05/1983	06:54:37.8	−13.8	171.3	27	−13.80	171.25	34	5.7 m_b	162
ISC	16/03/1984	06:09:01	−14.7	171.0	27	−14.65	171.00	17	4.8 m_b	18
ISC	29/06/1984	10:38:56.6	−14.2	171.0	49	−14.13	170.94	46	5.0 m_b	56
ISC	21/11/1984	14:33:19	−14.5	171.2	23	−14.49	171.18	16	5.7 m_b	205
ISC	21/11/1984	16:03:39.9	−14.5	171.1	12	−14.39	171.17	12	5.0 m_b	63
ISC	21/11/1984	18:17:50	−14.5	171.1	24	−14.49	171.04	13	5.5 m_b	173
TS	21/11/1984	19:16:56.3	−14.7	171.0	33	−14.63	170.93	21	4.9 m_b	26
ISC	23/11/1984	04:46:06	−14.3	171.3	33	−14.32	171.29	25	5.9 m_b	134
ISC	23/11/1984	07:12:30	−14.2	171.3	33	−14.12	171.32	20	5.4 m_b	115
ISC	06/12/1984	04:13:55	−14.5	171.0	33	−14.49	170.98	2	4.6 m_b	20
ISC	14/01/1985	22:06:25.2	−14.4	171.2	33	−14.29	171.21	10	4.9 m_b	33
HRV	25/12/1985	02:35:51.0	−14.1	170.0	33	−14.14	170.16	28	5.3 m_b	91
TS	12/11/1986	00:24:42.7	−13.9	168.8	33	−13.75	169.18	22	4.7 m_b	17
ISC	17/05/1988	14:25:56	−11.40	179.66	30	−11.51	170.68	53	5.7 m_b	200
ISC	22/06/1988	21:53:08	−15.21	168.20	26	−15.19	168.20	21	5.3 m_b	136
ISC	21/10/1988	08:51:43	−15.31	168.25	27	−15.33	168.25	25	5.2 m_b	105
TS	02/11/1989	02:21:58.4	−14.14	170.49	33	−14.04	170.48	10	5.2 m_b	54
TS	02/11/1989	03:40:27.7	−14.307	170.513	33	−14.06	170.51	10	5.1 m_b	13
ISC	08/11/1990	16:49:20	−14.05	170.51	33	−14.03	170.52	19	5.0 m_b	51
ISC	01/05/1991	00:59:50.4	−13.97	170.67	26	−13.91	170.63	23	4.9 m_b	41
ISC	11/05/1991	15:38:30	−13.32	168.78	23	−13.19	168.82	22	4.7 m_b	25
TS	09/11/1991	10:26:12.1	−13.054	175.668	33	−12.84	175.80	10	4.4 m_b	9
TS	29/11/1991	04:27:57.7	−14.995	171.454	33	−14.67	171.43	10	4.3 m_b	8
ISC	01/04/1992	19:38:47.2	−13.24	174.84	33	−13.17	174.73	46	5.2 m_b	100
ISC	18/10/1992	18:10:37.1	−14.07	176.71	34	−14.10	176.72	39	5.0 m_b	50
HRV	01/03/1993	20:47:46.8	−13.072	174.784	33	−12.79	175.16	15	5.3 M_w	32
HRV	03/03/1993	23:14:28.7	−13.342	175.009	13	−13.16	175.25	15	6.0 M_w	222
HRV	03/03/1993	13:06:27.9	−13.154	174.993	33	−13.13	175.00	15	5.3 M_w	49
TS	03/03/1993	14:11:29.9	−13.314	175.102	33	−13.35	175.12	35	4.9 m_b	32
ISC	03/03/1993	21:03:04.1	−13.164	174.910	11	−13.23	174.91	9	5.4 m_b	65
TS	04/03/1993	01:22:50.2	−13.312	174.917	33	−13.24	174.91	10	4.5 m_b	7
HRV	04/03/1993	14:36:00.3	−13.241	174.872	18	−13.11	174.94	15	5.7 M_w	187
TS	04/03/1993	14:53:14.0	−13.143	174.897	33	−13.07	174.87	10	4.8 m_b	13
HRV	04/03/1993	19:42:24.1	−13.253	175.007	33	−13.13	174.81	15	5.3 M_w	71
ISC	06/03/1993	10:59:14	−13.21	175.08	37	−13.23	175.10	37	5.3 m_b	48
TS	07/03/1993	22:04:45.8	−13.265	174.944	33	−13.31	174.98	31	4.8 m_b	29
TS	07/03/1993	22:18:16.9	−13.242	174.992	33	−13.25	175.02	36	4.9 m_b	30
TS	08/03/1993	12:04:29.0	−13.268	175.078	33	−13.19	175.08	10	4.8 m_b	13
TS	13/03/1993	07:46:12.2	−13.306	174.668	33	−13.27	174.78	5	4.9 m_b	14
HRV	28/03/1993	17:16:50.8	−13.114	175.001	33	−13.12	175.41	15	5.5 M_w	97
ISC	14/12/1993	07:49:58	−13.62	168.94	21	−13.61	168.94	7	5.2 m_b	90
ISC	03/04/1994	17:56:42.0	−15.03	168.23	25	−15.03	168.24	25	5.6 m_b	174
HRV	21/03/1996	15:43:15.0	−14.66	167.91	33	−14.51	167.93	15	5.6 M_w	88

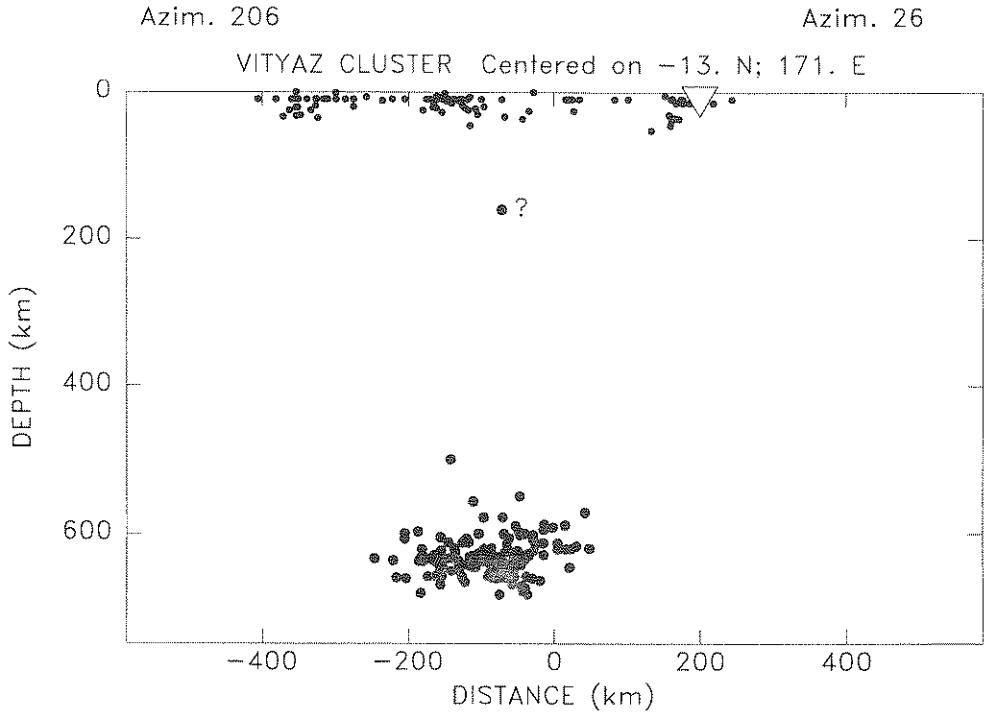

Fig. 7. Cross-section perpendicular to the Vityaz Trench (open triangle at zero depth), showing its relationship to the projected hypocenters of the Vityaz group of deep earthquakes. Question mark as in Fig. 6. Note general lack of seismological evidence for slab material between the trench and the deep earthquakes.

southernmost group of 5 earthquakes around 21.5°S and 175°E, while the Northern Finger can be prolonged along N266°E to the lone epicenter at 18°S; 173°E. Given the sparse level of seismicity along the North Finger, the latter association is admittedly tenuous. The former one appears much more definitive. The two remaining epicenters among the zone of scattered western deep seismicity could also align with some deep seismicity extending away from the base of the main WBZ at 18.7°S; 178°W.

Figs. 8 and 9 present cross-sections of the seismicity along these two fingers. Open symbols show the background seismicity in the WBZ. Since the two fingers are relatively discontinuous, it is not possible to assess their transverse dimension (in a direction perpendicular to the plane of the figures).

Fig. 8a shows that the hypocentral depths in the Southern Finger are constrained well above the worldwide depth of maximum seismicity, known to be 691 km (Stark and Frohlich, 1985; Rees and Okal, 1987; Okal and Bina, 1998), and approached in the Vityaz cluster. The depth at the tip of the finger is shallower than 600 km. However, two events along the finger reach 613 and 633 km, respectively. The deepest event is a shock with $m_b = 5.5$, well located by the ISC using 117 stations, and its depth (633 ± 4 km) cannot be contested. We conclude that the events at the tip of the finger are significantly shallower (by at least 40 km) than those in its center and as much as 190 km shallower than the bottom of the main WBZ. The finger curls back upwards towards its western tip. We also note that 8 out of the 22 events constituting the South Finger (including the two central deep ones) are part of a main shock–aftershock sequence extending over a period of 15 days in May–June 1986. Finally, other outboard events occur as much as 400 km west of the main WBZ at depths of 400 to 530 km (filled diamonds on Fig. 8a); their significance is discussed later.

3.4. Focal solutions

There are 11 CMT solutions available in the Vityaz cluster (Dziewonski et al., 1983 and subsequent quarterly updates), with relatively small moments ranging from 5.3×10^{23} to 2.1×10^{25} dyn-cm. In addition, two more solutions were obtained as part of the CMT inversions by Huang et al. (1997) of the WWSSN-era earthquakes. Finally, we were able to obtain two additional focal solutions (without associated scalar moments) from first motions read on WWSSN seismograms. The resulting 15 solutions are listed in Table 5, and shown in map view on Fig. 4. It is immediately apparent that a wide variety of mechanisms are present. Eight events, including the largest earthquakes in the group (13 Apr 1995 and 14 Dec 1992) do feature downwards compressional stress (their *P*-axis plunging 60° or steeper). The remaining seven range from mainly strike-slip to downwards tensional; no correlation is found with either depth or geographical location of the events. *T* and *N* axes show even greater scatter than *P*-axes.

Among the events west of the main Tonga WBZ, the only available CMT data consist of three solutions for the Southern Finger, two of them during the sequence of 1986 and the third further east towards the WBZ. In addition, Isacks and Molnar (1971) report a focal mechanism for the 01 Oct 1965 event inside the Fiji Basin. In the case of the 18 Nov 1970 event at the tip of the Southern Finger ($m_b = 5.6$), we obtained a focal solution through a combination of WWSSN picks and published ISC reports, which turned out to be remarkably consistent, and constrained the mechanism to a mostly strike-slip geometry. In turn, that mechanism provides an excellent fit to the ISC first-motion reports for the isolated event at the tip of the northern finger (26 Apr 1972; $m_b = 5.1$).

The resulting 21 focal mechanisms are listed in Table 5, which also includes the precursor to the 1986 Southern Finger main shock. Fig. 10 shows a compilation of stereographic projections of the orientation of the principal axes, and a comparison with their counterparts in the regular Tonga WBZ. We

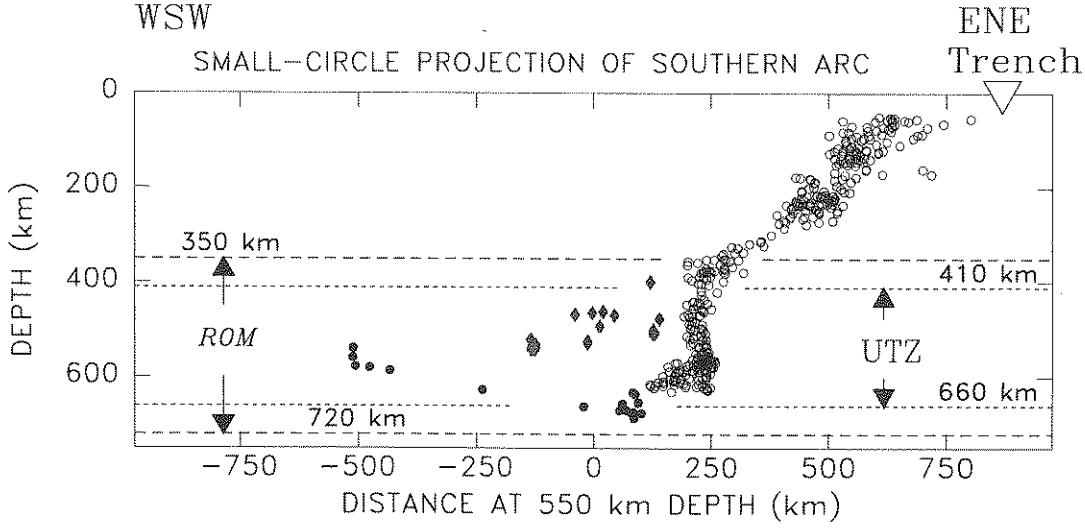

Fig. 8. (a) Cylindrical depth cross-section of the Southern finger group of outboard earthquakes (filled diamonds and circles) shown in Figs. 2 and 4; events in the main WBZ are shown as open circles. The section is along a small-circle arc centered at (43.5°S, 170°W). The dashed lines show the range of the transition zone in the unaltered mantle (UTZ) between 410 and 660 km, as well as the range of olivine metastability (ROM) in the slab, between 350 and 720 km. It is believed that the complex geometry of the deep WBZ reflects the resistance to slab descent into the transition zone and lower mantle, resulting in slab buckling and segmentation combined with the rapid eastward migration of the Tonga Trench. Such a process lays down slab and slab fragments in its wake. Note that many of the outboard earthquakes occur well above the 660 km discontinuity at the bottom of the transition zone and hence involve a mineralogical slab buoyancy and viscous resistance in the transition zone, not associated with descent into the lower mantle. (b) Tomographic image of the Southern Finger group of earthquakes slightly modified from Van der Hilst (1995). Section location similar, but not identical, to (a).

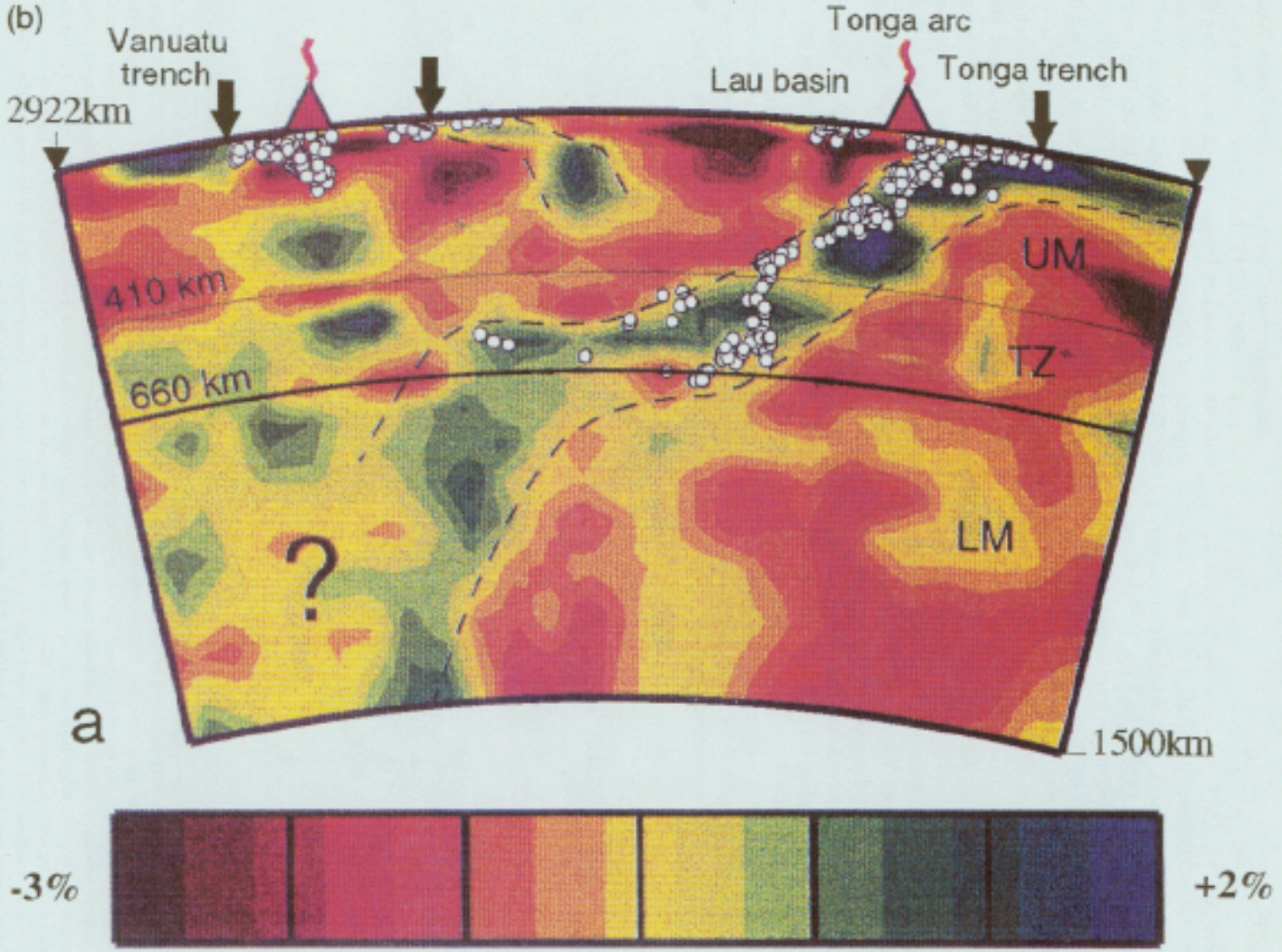

Fig. 8 (continued).

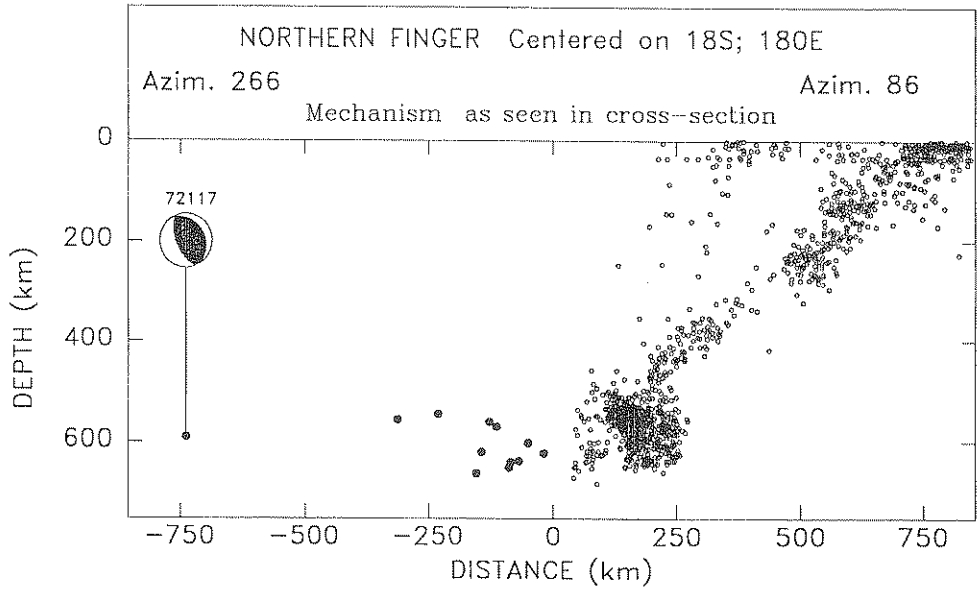

Fig. 9. Cross section parallel to the northern finger of outboard events west of the Tonga WBZ. The background seismicity of the Tonga trench between latitudes 17 and 19°S is shown by small open symbols. The focal mechanism shown for the westernmost outboard event is depicted as the back hemisphere would appear to an observer looking horizontally perpendicular to the plane of projection.

cannot uniquely define the geometry of stress release for the Vityaz and/or South Fiji events from this dataset. This is in contrast to the case of most subduction zones, where the overwhelming majority of the deepest events are found to release down-dip compressional stress, a conclusion first noted by Isacks and Molnar (1969), and upheld by later studies (e.g., Giardini, 1984). This phenomenology also applies to Argentina (bottom plots on Fig. 10), for which the lack of seismicity between 325 and 520 km had led early investigators to propose that the slab could be 'broken' with its deepest part mechanically separated from the upper one. The coherence of stress release in Argentina argues for a mechanically (if not seismically) continuous slab, a conclusion supported by tomography (Engdahl et al., 1995) and *T*-wave studies (Okal and Talandier, 1997). In contrast, the large scatter in focal solutions of the Vityaz group, and the lack of evidence for ongoing subduction are compatible with the idea of mechanically detached and possibly segmented seismogenic material.

A final note on the sizes of the events in the regions under study. We concluded above that the earthquakes are generally small, based on the Harvard catalogue. We strengthen this conclusion by noting that a comprehensive study of WWSSN seismograms (1962–1976) by Huang et al. (1997) revealed only two South Finger earthquakes in the study area of sufficient size ($M_0 = 2.5 \times 10^{25}$ dyn-cm) to permit moment-tensor inversion, as opposed to 29 more events for the whole Tonga WBZ system. Likewise, the study by Huang et al. (1998) of pre-WWSSN seismograms detected no event in our study area large enough to be inverted. Moment thresholds varied with time and location in that study but were as low as 1.6×10^{26} dyn-cm in this area.

4. Discussion

4.1. Plate provenances of the interarc deep earthquake zones

The complexity of the late-Cenozoic history of the broad interarc region between the Vanuatu and Tonga subduction zones (e.g., Barazangi et al., 1973; Brocher, 1985; Hamburger and Isacks, 1987, 1988; Greene et al., 1988; Louat et al., 1988; Yan and Kroenke, 1993) makes interpretation of the deep

Table 5
Focal mechanism and moment data

Source (†)	Date and origin time					Epicenter		Depth (km)	Moment	Focal mechanism			*P* axis		*T* axis	
	D	M	(J)	Y	HH:MM	°N	°E		dyn-cm	ϕ (°)	δ (°)	λ (°)	plunge	azimuth	plunge	azimuth
Vityaz Cluster																
a	10	4	(100)	1965	22:53	-13.45	170.30	641	3.3×10^{25}	66	76	197	22	289	2	199
a	4	11	(309)	1968	09:07	-14.20	172.02	578	6.9×10^{25}	18	32	285	74	66	14	277
b	4	5	(125)	1976	12:47	-13.88	172.61	602		306	69	252	62	188	22	50
b	19	5	(140)	1976	19:07	-12.79	169.24	647		325	60	208	40	181	4	274
c	17	3	(076)	1977	12:42	-12.92	168.97	649	8.1×10^{25}	325	54	195	34	179	16	280
c	31	10	(304)	1981	07:37	-12.70	169.00	650	7.8×10^{23}	216	43	293	4	142	74	37
c	13	2	(044)	1985	11:10	-13.07	168.91	637	5.3×10^{23}	282	21	260	11	337	19	71
c	7	9	(250)	1986	01:44	-12.88	169.80	671	7.9×10^{23}	23	28	255	71	147	18	304
c	24	9	(267)	1986	14:19	-13.87	173.08	635	2.7×10^{24}	248	49	181	28	104	27	210
c	6	8	(218)	1987	11:25	-12.66	168.86	628	9.2×10^{23}	318	39	165	26	178	41	294
c	15	4	(105)	1989	23:48	-13.69	171.89	575	2.7×10^{24}	80	37	168	28	298	40	55
c	14	12	(349)	1992	07:41	-13.99	170.87	642	3.4×10^{24}	305	38	278	81	357	8	209
c	12	3	(071)	1994	01:49	-14.50	171.09	612	1.5×10^{24}	151	66	83	21	247	68	47
c	13	4	(103)	1995	02:34	-13.45	170.43	637	2.1×10^{25}	109	48	254	78	306	1	210
c	2	12	(337)	1996	21:25	-13.98	170.37	628	2.2×10^{24}	296	50	310	60	273	2	179
North Finger																
b	26	4	(117)	1972	01:33	-18.23	173.01	591		60	75	200	24	283	3	192
Fiji Basin, between North and South Fingers																
d	1	10	(274)	1965	13:22	-19.89	174.46	541		85	85	306	39	28	31	147
South Finger																
b	18	11	(322)	1970	16:43	-21.81	175.23	576		60	75	200	24	283	3	192
c	27	7	(209)	1980	00:28	-19.57	179.64	554	1.5×10^{24}	42	73	1	11	357	13	265
c	26	5	(146)	1986	18:40	-21.57	-179.3	603	2.1×10^{26}	60	59	211	42	274	3	7
c	26	5	(146)	1986	19:06	-20.24	179.03	568	5.6×10^{26}	197	21	184	42	33	40	174
c	5	6	(156)	1986	00:17	-19.79	178.46	574	7.8×10^{23}	30	81	184	9	254	3	345

(†)a: Huang et al. (1997); b: This study; c: Dziewonski et al. (1983) and subsequent quarterly updates; d: Isacks and Molnar (1971).

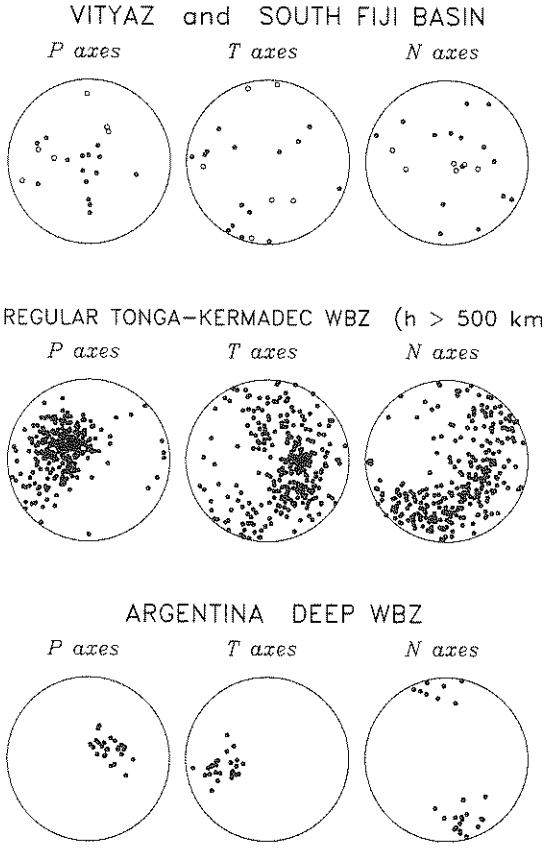

Fig. 10. Stereographic plots showing a compilation of the P, T and N directions for the focal mechanisms listed in Table 5. Top panels: Principal directions for the Vityaz (filled circles) and the outboard Tonga events beneath the South Fiji Basin (open circles). Central panel: The same for the Tonga–Kermadec events deeper than 500 km. Bottom panels: The same for the deep earthquakes beneath Argentina. Note the large scatter of these directions for the earthquakes under study compared to the ones for Tonga–Kermadec and Argentina.

earthquakes in that region difficult. Evidence for rapid back-arc spreading in the Lau and North Fiji Basins based on shallow seismicity (Hamburger and Isacks, 1987; Chen and Grimison, 1989; Eguchi et al., 1989), magnetic anomalies and marine geophysics (Malahoff et al., 1982; von Stackelberg and von Rad, 1990; Parson et al., 1990; Auzende et al., 1988, 1994; Parson and Hawkins, 1994) and satellite geodesy (e.g., Bevis et al., 1995) indicate that rapid trench migration and arc rotation are currently taking place at the Vanuatu and Tonga trenches. Reconstructions of trench positions back to 6–10 Ma b.p. based on analysis of magnetic anomalies in the Lau and North Fiji Basins implies a considerable change in subduction geometry since the time when the oceanic lithosphere presently at deep earthquake depths was originally subducted (e.g., Brocher, 1985; Auzende et al., 1988; Hamburger and Isacks, 1988). Marking the northern border of the North Fiji Basin is the Vityaz trench, a fossil convergent plate boundary continuous with the fossil North Solomon and the West Melanesian trenches, all thought to represent former southwestward subduction of the Pacific plate beneath the Australian plate up to late Miocene time, when a series of arc reversals occurred that initiated the current subduction regimes at the New Britain, Solomon and Vanuatu subduction zones (e.g., Hamburger and Isacks, 1987). Compounding the difficulty in reconstructing these motions are the shear deformations of the Fiji and Lau Basins shown by focal mechanisms of shallow earthquakes in those back-arc regions (Hamburger and Isacks, 1988; Eguchi et al., 1989). L.W. Kroenke (pers. comm., 1998) has suggested an intermediate episode of Northwestward subduction at the present location of the South Fiji Basin.

Hamburger and Isacks (1987) argue that most of the deep earthquakes between the Vanuatu and Tonga WBZs represent failure in slab material whose subduction geometry is not directly related to present-day active subduction in those two subduction zones. Our work supports this view. Considering the deep events of 15 Jan 1970 and 16 Sept 1976 as broadly a part of the Vityaz cluster, the latter extends under the Vanuatu WBZ. This spatial relationship re-enforces the interpretation that the deep slab material represented by Vityaz seismicity is not continuous with the present day Vanuatu slab (Barazangi et al., 1973; Hamburger and Isacks, 1987). This result and the rough parallelism of the ESE trend of the deep Vityaz cluster and that of the Vityaz trench support the analysis that those deep earthquakes are occurring in slab material originally subducted southwestward as the Pacific plate descended into the Vityaz trench and subsequently detached near the time of arc reversal.

The geometrical relations of the arc-shaped fingers of deep earthquakes that occur west of the

Tonga WBZ suggest that they are related to the past history of subduction at the Tonga trench via processes that are currently going on at the bottom of the Tonga zone. The North and South Fingers seem to be rooted to the east in the bottom of the Tonga WBZ. In fact, the Tonga zone seems to be depleted in earthquakes deeper than 600 km where the southern arc intersects the Tonga WBZ (Fig. 3). In other words, the deep structure of the arc-like band may be described as a tab-shaped feature with slab material missing in the Tonga WBZ at depths between 600–700 km near latitude 19–20°S, where the slab deflects westward as a nearly flat-lying tab. Similar but less well defined gaps may be seen at latitudes 22.5 to 23.3°S and 18.5 to 19°S where the deepest earthquake activity seems to be depleted at the bottom of the WBZ.

The roughly small-circle-arc shape is best defined for the finger-shaped band of events intersecting the Tonga WBZ near latitude 19.5°S and extending to longitude 175°E. Such a geometry is broadly consistent with failure occurring in slab material left stagnant in the transition zone along the expected arc-shaped migration path of the Tonga trench (Hamburger and Isacks, 1987; Bevis et al., 1995; Van der Hilst, 1995). Similar structures but with far shorter arc length may be found near latitudes 17.6, 18.7 and 23°S. Since these structures are largely rooted in depleted sectors of the deep Tonga Wadati–Benioff zone, the gap-and-tab geometry appears to apply to more than one sector of the deep Tonga slab.

Three well-located events (between 18 and 21°S and 173 and 175°E) may not fit this classification of deep earthquakes in the Vanuatu–Tonga interarc region. Because of the scarcity of deep activity in that region, we cannot rule out the possibility that those earthquakes are associated with failure in stagnant slab material laid down in the transition zone during the clockwise migration of the Vanuatu trench.

A similar interpretation is possible for the cluster of five deep shocks near 21.5°S; 175°E, although the alignment with the trend of the arc-shaped band to the ENE is suggestive of a relation to the Tonga system instead. Moreover, the high-wavespeed anomaly reported by Van der Hilst (1995) appears to resolve a continuous recumbent slab structure from the bottom of the inclined Tonga zone to the cluster in question.

If this interpretation of slab continuity is correct, then this southern arc-shaped band extends as much as 600 km WSW of its 'root' at the bottom of the Tonga WBZ. Estimates of the total amount of Tonga trench migration at present latitude 19–20°S vary greatly but bracket this number. They range from 300 km (estimated from the total back-arc extension implied by the separation of the Lau Ridge from the active Tonga arc ridge) to about 800 km estimated by extrapolating the GPS measurements of current rates of basin extension (Bevis et al., 1995) back to the time of initial opening of the Basin at 5.5–6 Ma b.p. (Parson and Hawkins, 1994; Hawkins, 1995). The first is an underestimate since it neglects the distributed extension of the Lau and Tonga Ridges.

It is worth noting that latitude 19°S also marks an important along-strike transition in the Tonga subduction zone: the youngest magnetic anomalies in the Lau Basin are segmented and the active spreading centers are offset by about 70 km near 19.5°S. The duration over which those spreading centers have operated differs greatly north and south of that boundary (Parson et al., 1990; Hawkins, 1995). Evident also are changes in the morphology of the active Tonga arc near 19.5°S. The short band of outboard deep earthquakes near latitude 22.7°S (Fig. 2) correlates with the southernmost end of the active Lau Basin spreading centers, the Valu Fa Ridge (Wiedicke and Collier, 1993). These relationships suggest that these along-strike variations in the rates of Tonga trench migration may somehow have played a role in the development of the bands of outboard deep earthquakes, perhaps by deforming the slab.

The anomalous seismic behavior evident where the arc-like bands of outboard earthquakes project back to gaps in the bottom of the Tonga zone suggests that the processes leading to the stagnation of the recumbent Tonga slab are ongoing. The complex structure at the base of the present Tonga WBZ points to the possibility that the slab material to the west is not continuous, but rather consists of complexly sheared slab fragments produced by exceptional resistance to slab penetration into the lower mantle and then laid down in the transition zone during trench migration. Below, we consider a conceptual model of the evolution of old and rapidly descending cold slabs that may help explain the above characteristics.

4.2. Thermo-kinetic and geodynamic implications of deep earthquakes in stagnant slabs

A number of fundamental questions concerning the inner workings of stagnant slabs are raised by the foregoing summary of deep seismicity beneath the North and South Fiji Basins and its plate-tectonics context. First, why are such events so much more abundant than elsewhere? Second, what is the origin of the deviatoric stresses in recumbent slab material that is stagnant in the transition zone? Third, by what process does deep seismogenic failure occur in such material? Fourth, why does the northern Tonga slab at least locally deflect to a recumbent attitude near the bottom of the transition zone and then, as suggested by the evolutionary model of Van der Hilst (1995), subsequently descend into the lower mantle?

Our initial approach is to consider only the purely thermal effects of slab descent. The Tonga slab, reflecting a combination of both rapid Pacific–Australia plate motion and rapid trench migration, is currently converging at 240 mm/yr near the northern end of the Tonga trench (McCaffrey, 1994; Bevis et al., 1995), a rate far greater than for any other subduction zone on Earth. Engebretson et al. (1991) and Engebretson (pers. comm., 1994) interpreted a series of ENE-trending magnetic lineations and NNW-trending fracture zones east of the Tonga trench as corresponding to the Phoenix lineations to the northwest, which implies their creation by Pacific–Phoenix spreading. They argue therefore that lithosphere currently just north of the Vityaz trench and east of the northern Tonga trench is formerly Phoenix-plate lithosphere (see also Joseph et al., 1993). If their interpretation is correct, then the lithosphere off the Tonga and Vityaz trenches is mid-to late anomaly M-series lithosphere, aged 150–160 Ma b.p.

Simple thermal conduction models for plate cooling and slab heating indicate that this combination of very old, cold lithosphere descending into the Tonga trench at very rapid rates should produce very cold slab thermal structure (e.g., Molnar et al., 1979; Stein and Stein, 1996). A recent numerical thermal model of the Tonga slab in a study by Kirby et al. (1996b) confirms this expectation: the slab can be more than 1000°C cooler than the surrounding mantle at depths exceeding 300 km. Although absolute temperatures from such models may have considerable uncertainties, it is almost inescapable that the combination of great plate age and fastest convergence rates for Tonga will produce the coldest thermal structure for any subducting slab in the Earth (see also discussion by Bevis et al., 1995).

Outboard Tonga events extend as much as 600–800 km west of the bottom of the WBZ. The occurrence of these earthquakes, in effect, lengthens the seismic zone and this extension helps us understand better an enigmatic feature of Tonga WBZ: even though the Tonga slab should be markedly colder than other slabs, the maximum depths of earthquakes in the Tonga WBZ are only 20–30 km deeper than the deepest earthquakes in other old, cold slabs. Using the arguments presented above, the total length of the cold seismogenic part of the Tonga slab should include the outboard bands of seismic activity, and hence is more in keeping with its expected colder thermal structure.

Similarly, lithosphere that subducted southward into the Vityaz trench 8 to 10 Ma ago would be expected to be of similar age to that presently entering the Tonga trench and having evidently sunk to the bottom of the transition zone following detachment about 8 Ma b.p., implying a free descent rate of at least 8 cm/a since the slab was detached.

Hence from these simple interpretations, both the active Tonga slab and the detached Vityaz slab are expected to be very cold and therefore strong, dense and more negatively buoyant compared to other slabs. The high level of seismic activity of the Tonga WBZ may well reflect this combination of high strength and presumably high slab stresses that derive from high density and large buoyancy forces combined with viscous or buoyancy forces resisting slab penetration into the lower mantle (e.g., Richter, 1979; Vassiliou and Hager, 1988; Bevis et al., 1995). Four related shortcomings make such a strictly thermal description of Tonga and Vityaz deep seismicity inadequate: (i) It does not explain how buoyancy-derived stresses can be significant in stagnated slab material lacking a continuous column of shallower slab above it; (ii) it does not explain why shear failure on faults can occur in slab material stagnated in the transition zone, regardless of the level of slab deviatoric stresses; (iii) it does not explain why the outboard Tonga earthquakes are typically much shal-

lower than the bottom of the transition zone at 660 km, where the forces expected to govern slab descent are thought to operate; and (iv) it ignores the thermophysical effects of mantle phase changes that must occur in slabs that enter the transition zone. We now consider how a recent model for deep earthquakes involving metastable mantle phase changes may be applied to extend this strictly thermal view of slabs and help remove those limitations (e.g., Kirby et al., 1996a).

Three recent independent studies have investigated the rates of transformation of olivine to spinel expected in descending slabs by combining models of heat conduction into slabs with laboratory-constrained kinetic theories (Kirby et al., 1996a; Dässler et al., 1996; Devaux et al., 1997). They show that for reasonable choices of slab thermal parameters, some degree of kinetic hindrance of the olivine-spinel reaction should occur when old, rapidly descending slabs enter the transition zone; thin, wedge-shaped regions of low-density peridotite should remain to depths greater than 600 km, depending on the calculated thermal structure. Although the depth extent of metastable peridotite wedges is sensitive to the details of the models and subject to considerable uncertainties, these studies agree that such metastable regions are at least plausible in old, cold slabs where deep earthquakes are generally found. Such a condition has several major consequences for slabs (Kirby et al., 1991, 1996a; Green and Houston, 1995).

4.2.1. Buoyancy effects of peridotite metastability

Regions of metastable peridotite contribute a positive buoyancy component that increases stepwise from $\approx 4\%$ at 440–550 km to 6.6% at 660 km and 13% at 740 km in the lower mantle (Fig. 11). This offsets to varying degrees the negative buoyancy accompanying the cold slab thermal structure (see Fig. 11). Thus the floating buoyancy 'cost' of metastable peridotite surviving inside cold slabs is significant at depths greater than 420 km and this cost doubles at depths greater than 660 km, making it difficult for slabs with appreciable peridotite to descend into the transition zone and the lower mantle and increasing the compressive stresses tending to buckle and deflect the coldest slabs when they enter the transition zone and especially when they reach its bottom. The buoyancy effect of peridotite metastability on slab morphology depends on the volume fraction of slab occupied and on the resistance to bending and slab dismemberment during deflection.

The probable existence in the slab of metastable olivine with a lower density than the mantle transition zone also helps us understand why many outboard earthquakes typically are much shallower than the depth to the bottom of the transition zone. The petrological buoyancy of metastable olivine in the transition zone may have permitted slab material deflected and laid down in the transition zone to actually reach neutral buoyancy or even float to shallower depths. Hence the petrological buoyancy of metastable peridotite may elevate, stabilize and stagnate the cold slab material in the transition zone west of the Tonga WBZ at depths shallower than the bottom of the transition zone at 660 km.

Bina (1996, 1997) has calculated the effects of the petrological buoyancy on slab stresses for both equilibrium phase boundaries and for a metastable peridotite wedge extending to about 650 km depth in a cold slab. He finds that in colder slabs, the downward deflection of the '660 km' discontinuity (i.e., the equilibrium $\gamma \rightarrow mw + pv$ transformation) to depths of the order of 700 km produces a deeper region of mineralogical buoyancy and larger compressive stresses than in warmer slabs. Richards and Wicks (1990) showed that the *S*-wave to *P*-wave conversions of rays propagating out the bottom of the northern Tonga slab are consistent with depressions of the '660 km' boundaries to such a depth. Bina has not performed stress calculations that incorporate the buoyancy forces from metastable peridotite that descends to depths greater than 660 km. The markedly larger density contrast with normal mantle of such material (Fig. 11) would produce even larger resistive forces than those produced by the equilibrium depression of the $\gamma \rightarrow mw + pv$ transformation. Thus the compressive slab stresses accompanying the persistence of metastable peridotite to depths greater than 660 km should be larger than those due to the effects of cold temperatures alone on the equilibrium mineralogy. This additional resistance to slab descent and the accompanying higher stresses in the coldest slabs may tend to produce more slab deformation and seismic activity and to buckle or offset them and hence arrest their descent into the lower mantle.

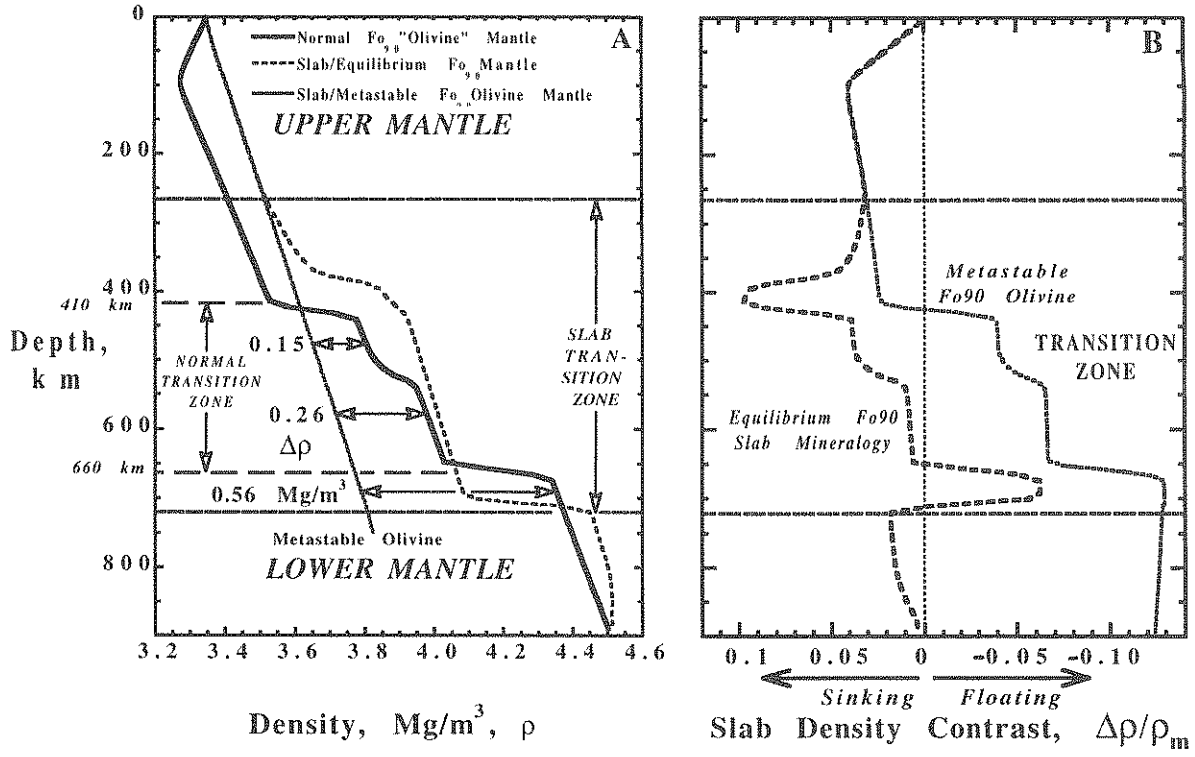

Fig. 11. (A) Variations of the mineralogical density distributions with depth for an olivine mantle composition of 90% Mg_2SiO_4 and 10% Fe_2SiO_4 in normal mantle (heavy solid line) and in a cold slab with an equilibrium mineralogy (dashed line) and with metastable olivine (dotted line). Data courtesy of Craig R. Bina from the model described in Bina (1996). (B) Density differences between normal mantle and a cold slab with an equilibrium (heavy dashed line) and a metastable olivine mineralogy (lighter dashed line). Note the large stepwise increases in the density differences for the metastable olivine case, especially at depths of about 420 and 660 km. Such density differences are believed to resist the descent of the coldest of slabs and prevent descent of such slabs into the lower mantle until the metastable olivine is largely consumed by the subsequent reaction to form spinel as the slab heats up by thermal conduction. This barrier to slab descent may cause the coldest slabs to stagnate temporarily in the transition zone and prevent earthquakes from occurring in the lower mantle (See Text).

4.2.2. Other effects of peridotite metastability

Variations in slab density associated with peridotite metastability would cause spatial and temporal variations of mineral and rock molar volumes; hence the presence of bodies of metastable peridotite in the transition zone is expected to produce internal non-hydrostatic stresses in slabs (see reviews in Kirby et al., 1991, 1996a). Stress fields of this type depend upon the geometries of the transformation boundaries as well as the rheologies of the relevant media. Stagnant slabs that are undergoing heterogeneous transformations from metastable peridotite to the transition-zone assemblage are expected to be subject to non-hydrostatic stresses of this type (Kirby et al., 1991, 1996a); we will discuss shortly the implications of such stresses in interpreting the occurrence and focal mechanisms of earthquakes in stagnant slabs where buoyancy-derived stresses may be less important than in inclined slabs.

Metastability of upper mantle rocks, both as anhydrous peridotite and serpentinized peridotite, also has implications for the seismogenic failure processes in deep slabs (see reviews by Green and Houston, 1995, Kirby, 1995 and Kirby et al., 1996a). Dehydration of hydrous phases elevates pore pressures and permits failure by brittle faulting at pressures far higher than expected in systems where fluids are not present (see review by Kirby et al., 1996b). Faults and fractures tend to be channels for hydrothermal fluids and localized hydrothermal alteration, such

faults created beneath the ocean basins may be reactivated when they dewater during conductive heating accompanying slab descent. Such a faulting mechanism has been suggested as the physical mechanism for intermediate and perhaps deep earthquakes (Silver et al., 1995; Kirby, 1995; Kirby et al., 1996b). Kirby et al. (1996a) argue that such faults are largely dewatered in slabs by depths of 300–350 km. However, should hydrous phases survive inside slabs descending into the transition zone, they would most likely do so inside regions of metastable peridotite where slabs are coldest. Another shear instability, termed transformational faulting, that occurs during rapid exothermic transformations in some mineral systems under metastable conditions, may be triggered in metastable peridotite as cold slabs descend into the transition zone (Kirby et al., 1985; Kirby, 1987; Green and Burnley, 1989; Kirby et al., 1991, 1996a; Green and Houston, 1995). The exothermic mineral transformations that are the best candidates for such faulting involve the dominant peridotite minerals: olivine → silicate spinel structure and enstatite → silicate ilmenite structure (Kirby et al., 1996a). A necessary condition for transformational faulting is the existence of metastable peridotite as a potential earthquake source region. Since lower-mantle-forming reactions are too slow and also strongly endothermic, the deep-earthquake population should by this mechanism be restricted to the depths of the mantle's transition zone, as modified by cold slab thermal structure (roughly 350 to 720 km), essentially as observed.

Thus there are three effects of possible peridotite metastability: slab buoyancy forces and associated stresses, self stresses from the heterogeneous volume changes and the existence of potentially seismogenic faulting processes. All have potential to help explain some previously enigmatic features of deep earthquakes in stagnant slabs, as detailed next.

4.3. An evolutionary model for the Tonga subduction zone

We interpret the above characteristics of outboard deep earthquakes beneath the Fiji Basin in terms of a three-stage evolutionary slab model (Fig. 12) described in very general terms in a recent paper by Kirby et al. (1996a).

(i) Rapid slab descent through the upper mantle and the formation of a metastable wedge in the very cold slab as it enters the transition zone. The cold slab descends to depths exceeding 660 km where the buoyant metastable olivine and the buoyancy associated with the depression of the $\gamma \rightarrow mw + pv$ transformation augment the resistance to descent below 660 km caused by increased viscosity. These sources of stress and the self stresses resulting from the volume changes activate faulting in the transition zone by dehydration embrittlement or by transformational faulting. Rapid descent rates are sustained by the large thermal buoyancy of the slab in the upper mantle. The large resistive forces that attend the petrological buoyancy at 660–690 km temporarily and locally stall the slab descent there and produce exceptionally high slab strain rates. The slab buckles and/or is mechanically disrupted into segments as resistance to descent into the lower mantle increases with increasing depth. The shallower inclined slab is free to migrate oceanward and the deep slab is thus deflected to a sub-horizontal geometry and offset from its former position to the west. As expected, the rate and maximum depth of seismic deformation and hence the frequency of occurrence of deep earthquakes are larger than for ordinary slabs.

(ii) Deep earthquakes continue to occur in the metastable peridotite within the offset or recumbent slab segments in response to the self stresses that accompany the volume change as it heats up and transforms to transition-zone rock. The deformation geometry revealed by the focal mechanisms of these earthquakes is complex because their thermal states, internal phase boundaries and self stresses are also complex. Such earthquakes tend to be smaller than in the main Tonga WBZ because the segmented metastable peridotite source regions are likely to be smaller than in intact slabs. Those slab segments can float to shallower depths if their net buoyancy is positive and large enough to overcome the viscous forces resisting ascent. Earthquakes in such segments therefore tend to be shallower that the events at the base of the main Tonga WBZ.

(iii) As the slab segments heat up by thermal conduction, more and more peridotite is consumed by the reaction to form spinel. After sufficient buoyant metastable peridotite is consumed, the slab fragments attains negative buoyancy sufficient to sink

below 660 km where it transforms to *mw* + *pv* and descends slowly into the lower mantle.

4.3.1. Applications to the Vityaz system

Similarities in the size distributions and focal mechanisms of events in the Vityaz and outboard Tonga groups suggest that the present model may also help explain some aspects of the deep seismic activity of the Vityaz group. The great age of lithosphere North of the Fiji Basin and Vityaz Trench and the possibility of rapid free descent of the detached Vityaz slab may have caused it to be very cold. However, lack of detailed knowledge of the history of detachment of the former Pacific plate and its subsequent descent into the transition zone bars any confident assessment of the present thermophysical state of that stagnant Vityaz slab. The Vityaz group of deep earthquakes is broadly *M*-shaped in map view, elongated roughly parallel to the nearby Vityaz trench, and about 200 km distant from that feature. Its breadth in the NNE direction is about 200 km and its thickness less than 100 km, suggesting that it is in a nearly horizontal attitude.

Two obvious differences exist between the outboard Tonga earthquakes and those in the Vityaz group. Most of the events in the Vityaz group are deeper than 620 km and many occur at depths between 630 and 650 km. These shocks are significantly deeper than most of the outboard events west of Tonga. They are also far more abundant. These

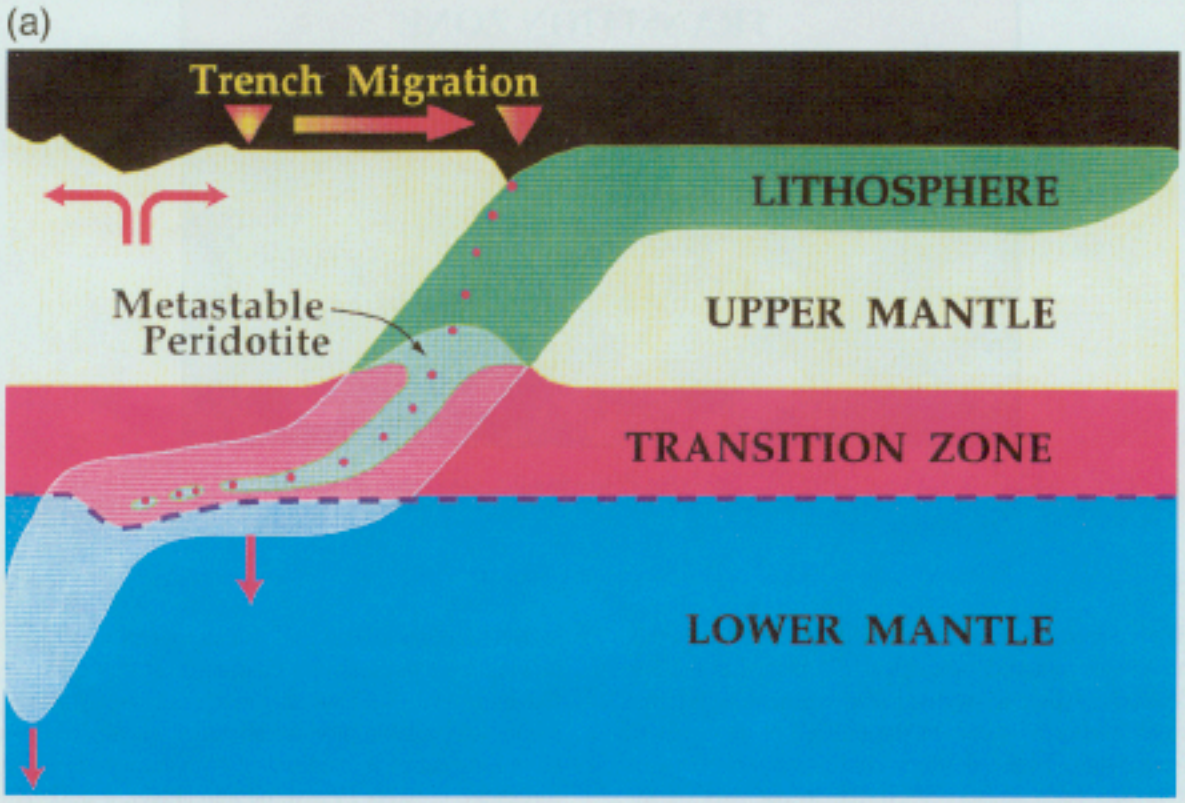

Fig. 12. (a) Schematic diagram showing hypothetical mineralogical structures of the inclined Tonga slab and its stagnant recumbent extension (adapted from the cartoon in Lay (1995)). The high buoyancy cost of subducting metastable olivine into the lower mantle stalls the bottom of the Tonga slab, causes it to buckle and segment as such material is laid down during eastward trench migration. The slab resumes descent when it has transformed to spinel and then to magnesiowüstite plus perovskite. (b) Schematic diagram showing hypothetical mineralogical structures of the detached Vityaz slab. Locations of intraslab earthquakes are shown as red asterisks. The detached slab is more intact than the one in (a) and the metastable olivine has been partially consumed, so that the remaining part of the slab has resumed negative buoyancy and foundered to the bottom of the transition zone.

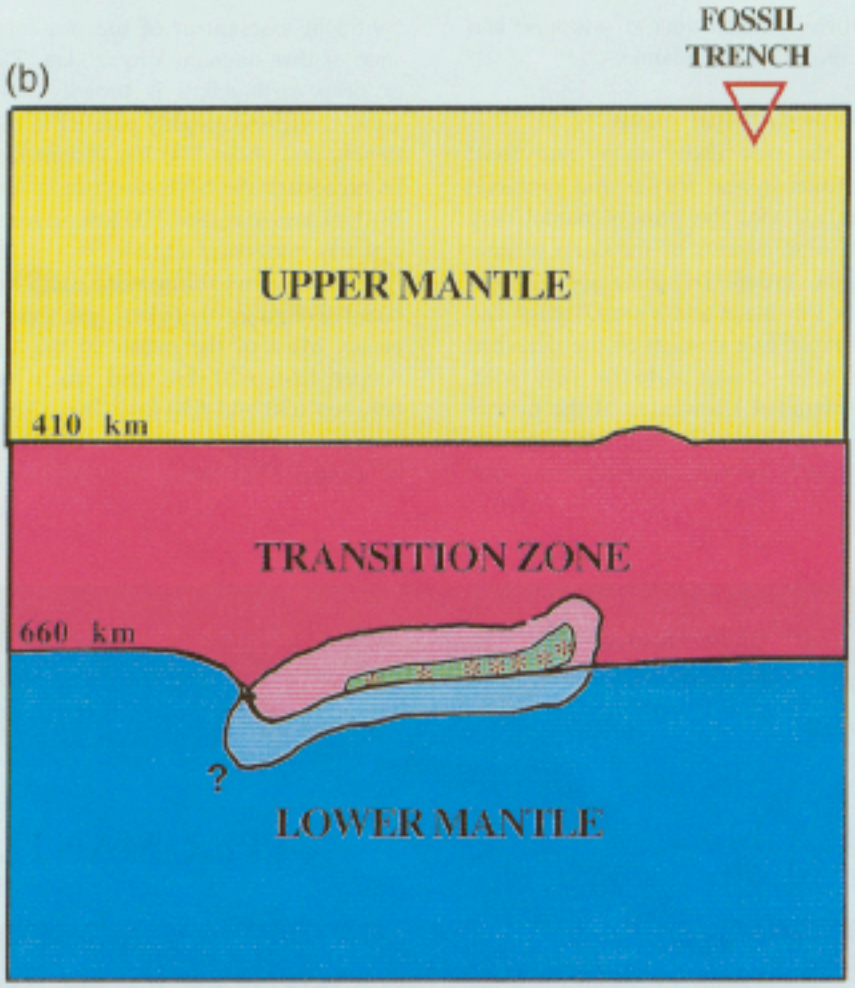

Fig. 12 (continued).

differences are not understood. One possibility is that the Vityaz slab, having evidently detached in the late Cenozoic, was not mechanically segmented like that which currently occurs at the bottom of the inclined Tonga slab, hence a more continuous seismogenic zone has been preserved. If the lower part of the Vityaz slab has already transformed to spinel and been partially assimilated into the lower mantle, it may have acquired an average density exceeding the ambient density of the bottom of the transition zone and thus could have foundered by gravity to the bottom of the zone.

Because geological and seismological evidence is lacking for a present-day continuity of this evidently flat-lying slab with an inclined shallower slab segment, appreciable non-hydrostatic stresses derived from long-range transmittal of buoyancy and viscous forces are unlikely (Vassiliou and Hager, 1988). This again points to the possibility that self stresses derived from complex kinetic phase boundaries of metastable peridotite may induce those shocks. The complex focal mechanisms of those earthquakes are in keeping with the complex states of self stress expected from such a condition. Since there are no

events with well determined magnitudes greater than 6.0, this limits any circular seismic source region dimensions to less than about 10 km, consistent with a small dimension of a segmented metastable peridotite seismogenic zone (Okal and Kirby, 1995).

5. Summary and conclusion

The Earth's most active zone of deep seismic faulting in stagnant slabs occurs in the transition zone between the Vanuatu and Tonga subduction zones and beneath the Fiji Basin. We have conducted a comprehensive survey of these earthquakes by systematically relocating them using a consistent methodology and have summarized new and published focal mechanisms. Based on this work, we recognize two groups of such earthquakes: the Vityaz group south of the fossil Vityaz trench and a group west and hence outboard of the Tonga Wadati–Benioff zone that occur in arc-shaped, diffuse, and discontinuous bands rooted near the bottom of the Tonga zone. Prior work has suggested that the slab material in which these groups formed was created by somewhat different processes: the Vityaz group represents a detached slab evidently created by a Late Miocene arc reversal and the outboard Tonga group represents material laid down in the transition zone during rapid Tonga trench rollback. Seismic tomography indicates that this recumbent slab material subsequently sinks into the lower mantle further west where it is aseismic. The earthquakes in these two groups are generally small (with magnitudes less than 6) and their focal mechanism are complex and unlike those in either at the nearby Vanuatu or Tonga Wadati–Benioff zones. The arc-shaped bands of outboard earthquakes project back to depleted zones in the bottom of the Tonga WBZ, producing a tab-and-gap structure. We develop an evolutionary model for the Tonga slab that incorporates the concept of kinetic hindrance of cold slabs as they enter the transition zone, metastable persistence of peridotite as a wedge-shaped structure in the inclined slab with failure by faulting taking place in the metastable peridotite associated with phase changes. The slab deflects at the bottom of the transition zone due to viscous resistance and to the buoyancy forces associated with metastable peridotite and cold spinel. Seismic failure may then be activated in the remaining bodies of peridotite by stresses caused by the volume changes that take place as they are slowly consumed by transformation to transition zone minerals. When metastable peridotite is thus largely consumed, the buoyancy force becomes more negative and the slab can sink and transform into the lower mantle assemblage, seismically because metastable peridotite is no longer present.

The outboard earthquakes are not in a continuous sheet west of the Tonga WBZ but rather arranged in discontinuous bands. These bands correspond in latitude to along-strike variations in the amount, style and rates of back-arc spreading. This suggests to us that the seismic banding of outboard events may reflect the slab deformation effects of a segmented trench migration and the westward flow of transition-zone mantle material under the Tonga slab to accommodate trench migration.

Likewise, deep seismic failure can occur in cold detached slab material if it sinks fast enough into the transition zone to retain appreciable bodies of metastable peridotite. As it stagnates after sinking to the bottom of the transition zone, it can continue to deform by an accommodation of the volume change associated with the transformation of peridotite to transition-zone minerals. The properties of the deep earthquakes that we investigated are in general accord with the speculative evolutionary model outlined above.

Acknowledgements

We thank David Engebretson, Seth Stein, and Paul Lundgren for valuable discussion, Bob Engdahl for access to his relocation catalogue prior to publication, and Rob van der Hilst for permission to use his published tomographic images. Robin Adams kindly provided the optimized beams of the 1983 event at WRA. Craig Bina provided the density data for Fig. 11. EAO acknowledges the support of NSF Grant EAR-93-16396.

Appendix A. The case of the intermediate-depth event of 16 May 1983

We present here a detailed analysis of this earthquake, which could not be relocated into the known

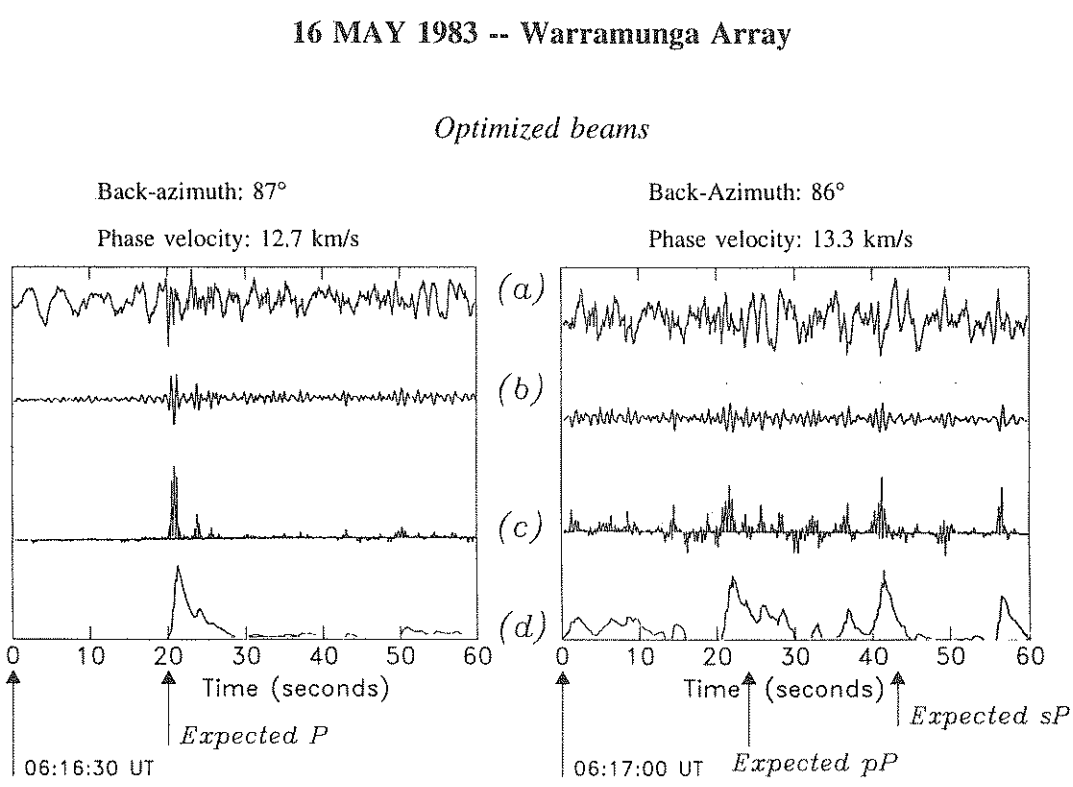

Fig. 13. Optimized beam seismograms at Warramunga Array for the intermediate-depth earthquake of 16 May 1983. Both windows around the P arrival (left) and the reflected pP and sP phases (Right) are processed. (a): Full optimized beam; (b): Beam filtered between 1 and 2 Hz; (c): Cross-correlogram of (b); (d): Cross-correlogram of (b) integrated over 1.5 s windows. Courtesy of Dr. Robin Adams.

seismic provinces (Vanuatu Trench; deep Vityaz cluster; shallow Fiji Basin...), and could be an intermediate-depth event located above the Vityaz cluster.

The ISC entry is reproduced on Fig. 13. Only eight stations reported travel times, of which two are close neighbors (WB2 and WRA). While this number is of course very low, we note a reasonable distance coverage, with in particular CHG at 76°. Our solution (based on the 8 available P times and shown on Fig. 13), the ISC hypocenter and the NEIC solution all fall within a few km of each other. With a standard deviation of residuals of only $\sigma = 0.77$ s, the quality of our solution is excellent. The epicenter is about 220 km away from events of similar depths in the Vanuatu WBZ. In order to further probe the location of this event, we conducted the following tests.

* We arbitrarily deleted one station from the dataset; as shown on Fig. 13, all eight possible relocations based on 7 P times converge at depths ranging from 152 to 169 km. Not surprisingly, deletion of the station with the highest importance, CHG, moves the epicenter the farthest (about 100 km), but actually to the northeast, away from the Vanuatu slab.

Fig. 14. Relocation of the intermediate depth event of 16 May 1983. Top: Copy of the event's ISC entry. Bottom: Result of relocation using the algorithm of Wysession et al. (1991). The 'importance' parameter follows the definition of Minster et al. (1974). The last 8 entries represent a bootstrapping procedure designed to test the robustness of the solution with respect to the deletion of one station. Note that the removal of even the most important station (CHG) has practically no effect on the solution.

16 May 1983

NEIS 16d 06h 10m 20s ± 1s, 12.9°S × 169.0°E, h 162km, Mb3.7, Poor solution.

ISC 16d 06h 10m 19s ± 1s6, 12.83S ± .091 × 169.1E ± .16
h 162km ± 7.1km, n8, σ 1s11/8, Mb3.8/1, 1D, Santa Cruz Islands region

PVC	**Port Vila**	**4.94**	**189 cP**	**06 11 32.0**	**−0.9**
PVC	Port Vila		*i*S	06 12 28.8	−1
HNR	**Honiara**	**9.62**	**290 *e*P**	**06 12 34.0**	**−1.0**
HNR	Honiara		*e*S	06 14 05.0	−16
NOU	**Nouméa**	**9.76**	**195 cP**	**06 12 38.0**	**+1.2**
NOU	Nouméa		*i*S	06 14 11.8	−13
SVO	**Savo**	**9.84**	**291 *e*P**	**06 12 39.0**	**+1.1**
SVO	Savo		*e*S	06 13 13	−74
CTAO	**Charters Towers**	**23.07**	**249 P**	**06 15 11.9**	**+0.4**
WB2	**Warramunga Ar**	**34.05**	**253 P**	**06 16 49.6**	**−0.5**
WRA	**Warramunga Ar**	**34.06**	**253 ↓P**	**06 16 49.8** *(.3)*	**−0.4**
CHG	**Chieng Mai**	**75.96**	**293 *e*P**	**06 21 50.8**	**+0.3**

```
Iteration #10   -12.84   169.14   d =  160.4 km; H-zero =    6:10:19.0
    8 stations less than 102 degrees away
standard deviation =       0.77   seconds.
station, distance, dt/ddelta, residual, importance
PVC    P      4.95      13.19      -0.85      0.646
HNR    P      9.63      13.00      -0.95      0.495
NOU    P      9.79      13.00       1.07      0.419
SVO    P      9.86      13.00       1.08      0.498
CTA    P     23.08       9.60       0.42      0.402
WB2    P     34.05       8.50      -0.56      0.292
WRA    P     34.07       8.50      -0.45      0.292
CHG    P     75.98       5.60       0.24      0.956

WITHOUT PVC (P) -12.85   169.00   d =  169.3 km; H-zero =    6:10:20.8
    7 stations less than 102 degrees away
standard deviation =       0.62   seconds.

WITHOUT HNR (P) -12.88   169.18   d =  166.6 km; H-zero =    6:10:19.4
    7 stations less than 102 degrees away
standard deviation =       0.64   seconds.

WITHOUT NOU (P) -12.89   169.13   d =  158.8 km; H-zero =    6:10:18.9
    7 stations less than 102 degrees away
standard deviation =       0.62   seconds.

WITHOUT SVO (P) -12.78   169.11   d =  152.2 km; H-zero =    6:10:18.3
    7 stations less than 102 degrees away
standard deviation =       0.58   seconds.

WITHOUT CTA (P) -12.87   169.08   d =  162.8 km; H-zero =    6:10:19.6
    7 stations less than 102 degrees away
standard deviation =       0.79   seconds.

WITHOUT WB2 (P) -12.82   169.17   d =  157.4 km; H-zero =    6:10:18.6
    7 stations less than 102 degrees away
standard deviation =       0.78   seconds.

WITHOUT WRA (P) -12.82   169.16   d =  158.0 km; H-zero =    6:10:18.7
    7 stations less than 102 degrees away
standard deviation =       0.79   seconds.

WITHOUT CHG (P) -12.38   169.99   d =  158.7 km; H-zero =    6:10:10.4
    7 stations less than 102 degrees away
standard deviation =       0.70   seconds.
```

* We conducted a series of 400 Monte Carlo relocations after injecting Gaussian random noise ($\sigma_G = 1$ s) into the arrival times; the resulting ellipse is elongated in the NE–SW direction, but its most extreme points remain at least 150 km away from the WBZ. Even doubling the amplitude of the noise to 2 s, a value unrealistic for an earthquake in the 1980s, fails to extend the ellipse to the WBZ. Similarly, the Monte Carlo depths are very stable: they range from 132 to 183 km ($\sigma_G = 1$ s), and from 97 to 215 km ($\sigma_G = 2$ s). In conclusion, the Monte Carlo tests confirm that the event is neither shallow, nor in the nearby Vanuatu WBZ.

* The best shallow location (h constrained to 10 km) achieves a mediocre standard deviation of the residuals ($\sigma = 4.1$ s), and a deep location (h constrained to 600 km) is even worse ($\sigma = 22.6$ s). The earthquake can be interpreted neither as a shallow event in the Fiji Basin, nor as a member of the deep Vityaz cluster.

* Of the four S times listed in the ISC entry, the fast arrivals at NOU and HNR (16 and 13 s early) may be due to travel inside the Vanuatu and Solomon slabs; S times are notoriously variable in such environments (Frohlich and Barazangi, 1980). The exceedingly negative residual at SVO (-74 s) probably results from misidentification of the phase sP_n, according to the iaspei91 model (Kennett and Engdahl, 1991).

* A solution in the Vanuatu Trench can be achieved by disregarding station CHG, but including in the dataset the S times at NOU and HNR. However, this solution is of poor quality ($\sigma = 2.61$ s); furthermore, it is controlled by the questionable S times, and as described above, moves east if only the subset of P times is used.

* Fig. 14 shows a record of the optimized beam from the Warramunga, Australia (WRA) array [courtesy of Dr. Robin Adams]. Note that this procedure identifies two correlations ≈ 30 s and 50 s after the main P arrival, from a back-azimuth of 86° and with a slowness of 0.075 s/km (8.36 s/deg). The agreement with parameters expected of the phases pP and sP for a source depth of 160 km (34 s, 8.69 s/deg; 53 s, 8.66 s/deg, respectively, the computed back-azimuth being 84°) is comparable to that for the main P phase (beamed back-azimuth 87°; beamed slowness: 8.75 s/deg; computed slowness: 8.57 s/deg). The time delays pP-P and sP-P would suggest a somewhat shallower source (140 to 150 km). Thus, the evidence for intermediate depth from primary travel times is strongly supported by beam optimization at the Warramunga array.

In conclusion, we could not find an acceptable solution except at an intermediate depth. A solution in the Vanuatu Trench cannot be totally discounted, but its quality is low, and it has to rely on regional S times, which are unreliable in this tectonic environment.

References

Adams, R.D., 1963. Source characteristics of some deep New Zealand earthquakes. N.Z. J. Geol. Geophys. 6, 209–220.

Adams, R.D., Ferris, B.G., 1976. A further earthquake at exceptional depth beneath New Zealand. N.Z. J. Geol. Geophys. 19, 269–273.

Anderson, H., Jackson, J., 1987. The deep seismicity of the Tyrrhenian Sea. Geophys. J. Roy. Astr. Soc. 91, 613–637.

Anderson, H., Webb, T., 1994. New Zealand seismicity: patterns revealed by the upgraded national network. N.Z. J. Geol. Geophys. 37, 477–493.

Auzende, J.-M., Eissen, J.-P., Lafoy, Y., Gente, P., Charlou, J.-L., 1988. Seafloor spreading in the North Fiji Basin (Southwest Pacific). Tectonophysics 146, 317–351.

Auzende, J.-M., Pelletier, B., Lafoy, Y., 1994. Twin active spreading ridges in the North Fiji Basin (Southwest Pacific). Geology 22, 63–66.

Barazangi, M., Isacks, B.L., Oliver, J.E., Dubois, J., Pascal, G., 1973. Descent of lithosphere beneath New Hebrides, Tonga–Fiji and New Zealand: evidence for detached slabs. Nature 242, 98–101.

Bevis, M., Taylor, F.W., Schutz, B.E., Recy, J., Isacks, B.L., Helu, S., Singh, R., Kendrick, E., Stowell, J., Taylor, B., Calmant, S., 1995. Geodetic observations of very rapid convergence and back-arc extension at the Tonga arc. Nature 374, 249–251.

Bina, C.R., 1996. Phase transition buoyancy contributions to stresses in subducting lithosphere. Geophys. Res. Lett. 23, 3563–3566.

Bina, C.R., 1997. Patterns of deep seismicity reflect buoyancy stresses due to phase transitions. Geophys. Res. Lett. 24, 3301–3304.

Brocher, T.M., 1985. On the formation of the Vitiaz trench lineament and North Fiji Basin. In: Brocher, T.M. (Ed.), Geological Investigations of the Northern Melanesian Borderland. Circum-Pacific Council for Energy and Mineral Resources, Houston, 1985, Earth Sciences Series, Vol. 3, pp. 13–33.

Buforn, E., Udias, A., Madariaga, R., 1991. Intermediate and deep earthquakes in Spain. Pure Appl. Geophys. 136, 375–393.

Chen, W.-P., Grimison, N.L., 1989. Earthquakes associated with diffuse zones of deformation in the oceanic lithosphere: some examples. Tectonophysics 166, 133–150.

Chung, W.-Y., Kanamori, H., 1976. Source process and tectonic implication of the Spanish deep-focus earthquake of March 29, 1954. Phys. Earth Planet. Inter. 13, 85–96.

Daässler, R., Yuen, D.A., Karato, S.-i., Riedel, M.R., 1996. Two-dimensional thermo-kinetic model for the olivine-spinel phase transition in subducting slabs. Phys. Earth Planet. Inter. 94, 217–239.

Devaux, J.-P., Schubert, G., Anderson, C., 1997. Formation of a metastable olivine wedge in a descending slab. J. Geophys. Res. 102, 24627–24637.

Dziewonski, A.M., Friedman, A., Giardini, D., Woodhouse, J.H., 1983. Global seismicity of 1982: centroid moment tensor solutions for 308 earthquakes. Phys. Earth Planet. Inter. 33, 76–90.

Eguchi, T., Fujinawa, Y., Ukawa, M., 1989. Microearthquakes and tectonics in an active back-arc basin: the Lau Basin. Phys. Earth Planet. Inter. 56, 210–229.

Engdahl, E.R., Van der Hilst, R.D., Berrocal, J., 1995. Imaging of subducting lithosphere beneath South America. Geophys. Res. Lett. 22, 2317–2320.

Engdahl, E.R., Van der Hilst, R., Buland, R.P., 1997. Global teleseismic earthquake relocation with improved travel times and procedures for depth determination, Bull. Seismol. Soc. Am., submitted.

Engebretson, D.C., Mammerickx, J., Raymond, C.A., 1991. Tonga lineations—the Phoenix plate has arisen?. Eos, Trans. Am. Geophys. Un. 72 (44), 444, [abstract].

Frepoli, A., Selvaggi, G., Chiarabba, C., Amato, A., 1996. State of stress in the Southern Tyrrhenian subduction zone from fault-plane solutions. Geophys. J. Int. 125, 879–891.

Frohlich, C., Barazangi, M., 1980. A regional study of mantle velocity variations beneath Eastern Australia and the Southwestern Pacific using short-period recordings of *P*, *S*, *PcP* and *ScS* waves produced by Tongan deep earthquakes. Phys. Earth. Planet. Inter. 21, 1–14.

Fukao, Y., Obayashi, M., Inoue, H., Nenbai, M., 1992. Subducting slabs stagnant in the mantle transition zone. J. Geophys. Res. 97, 4809–4822.

Giardini, D, 1984. Systematic analysis of deep seismicity: 200 centroid-moment tensor solutions to earthquakes between 1977 and 1980. Geophys. J. Roy. Astr. Soc. 77, 883–911.

Giardini, D., Velonà, M., 1991. The deep seismicity of the Tyrrhenian Sea. Terra Nova 3, 57–64.

Giardini, D., Woodhouse, J.H., 1984. Deep seismicity and modes of deformation in Tonga subduction zone. Nature 307, 505–509.

Giardini, D., Woodhouse, J.H., 1986. Horizontal shear flow in the mantle beneath the Tonga Arc. Nature 319, 551–555.

Green, H.W. II, Burnley, P.C., 1989. A new self-organizing mechanism for deep earthquakes. Nature 341, 733–737.

Green, H.W. II, Houston, H., 1995. The mechanics of deep earthquakes. Annu. Rev. Earth Sci. 23, 169–213.

Greene, H.G., Macfarlane, A., Johnson, D.P., Crawford, A.J., 1988. Structure and tectonics of the central New Hebrides arc. In: Greene, H.G., Wong, F.L (Eds.), Geology and Offshore Resources of Pacific Island Arcs; Vanuatu Region. Circ. Pac. Counc. Energy Miner. Res., Vol. 8, pp. 377–412.

Gutenberg, B., Richter, C.F., 1938. Depth and geographical distribution of deep-focus earthquakes. Geol. Soc. Am. Bull. 49, 249–288.

Gutenberg, B., Richter, C.F., 1939. Depth and geographical distribution of deep-focus earthquakes (2nd paper). Geol. Soc. Am. Bull. 50, 1511–1528.

Gutenberg, B., Richter, C.F., 1949. Seismicity of the Earth and Associated Phenomena, 2nd edn. Princeton Univ. Press, 273 pp.

Hamburger, M.W., Everingham, I.B., 1986. Seismic and aseismic zones in the Fiji region. Bull. Roy. Soc. N.Z. 24, 439–453.

Hamburger, M.W., Isacks, B.L., 1987. Deep earthquakes in Southwest Pacific: a tectonic interpretation. J. Geophys. Res. 92, 13841–13854.

Hamburger, M.W., Isacks, B.L., 1988. Diffuse back-arc deformation in the Southwest Pacific. Nature 332, 599–604.

Hawkins, J.W., 1995. Evolution of the Lau Basin—insights from ODP Leg 135. Am. Geophys. Un. Geophys. Monogr. 88, 125–173.

Huang, W.-C., Okal, E.A., Ekström, G., Salganik, M.P., 1997. Centroid-moment-tensor solutions for deep earthquakes predating the digital era: the WWSSN dataset (1962–1976). Phys. Earth Planet. Inter. 99, 121–129.

Huang, W.-C., Okal, E.A., Ekström, G., Salganik, M.P., 1998. Centroid moment tensor solutions for deep earthquakes predating the digital era: the historical dataset (1907–1961). Phys. Earth Planet. Inter. 106, 181–190.

Isacks, B.L., Molnar, P., 1969. Mantle earthquake mechanisms and the sinking of the lithosphere. Nature 223, 1121–1124.

Isacks, B.L., Molnar, P., 1971. Distribution of stresses in the descending lithosphere from a global survey of focal mechanism solutions of mantle earthquakes. Rev. Geophys. 9, 103–174.

Isacks, B.L., Sykes, L.R., Oliver, J., 1967. Spatial and temporal clustering of deep and shallow earthquakes in the Fiji–Tonga–Kermadec region. Bull. Seismol. Soc. Am. 57, 935–958.

Isacks, B.L., Sykes, L.R., Oliver, J.E., 1968. Seismology and the new global tectonics. J. Geophys. Res. 73, 5855–5899.

James, D.E., Snoke, J.A., 1990. Seismic evidence for continuity of the deep slab beneath Central and Eastern Peru. J. Geophys. Res. 95, 4989–5001.

Joseph, D., Taylor, B., Shor, A.N., 1993. The Nova–Canton Trough and the Late Cretaceous evolution of the Central Pacific. In: Sager, W.W., Sliter, W.V., Stein, S. (Eds.), The Mesozoic Pacific; Geology, Tectonics, and Volcanism. Am. Geophys. Un. Geophys. Monogr., Vol. 77, pp. 171–185.

Kennett, B.L.N., Engdahl, E.R., 1991. Travel times for global earthquake location and phase identification. Geophys. J. Int. 105, 429–465.

Kirby, S.H., 1987. Localized polymorphic phase transitions in high-pressure faults and applications to the physical mechanism of deep earthquakes. J. Geophys. Res. 92, 13789–13800.

Kirby, S.H., 1995. Intraslab earthquakes and phase changes in

subducting lithosphere. US Natl. Rept. Intl. Un. Geod. Geophys., Revs. Geophys. 33, 287–297.

Kirby, S.H., Durham, W.B., Heard, H.C., 1985. Rheology of ices I_h, II and III at high pressures: a progress report. In: Klinger, J., et al. (Eds.), Ices in the Solar System. Reidel, Norwell, MA, pp. 711–729.

Kirby, S.H., Durham, W.B., Stern, L.A., 1991. Mantle phase changes and deep-earthquake faulting in subducting lithosphere. Science 252, 216–225.

Kirby, S.H., Stein, S., Okal, E.A., Rubie, D., 1996a. Deep earthquakes and metastable mantle phase transformations in subducting oceanic lithosphere. Rev. Geophys. Space Phys. 34, 261–306.

Kirby, S.H., Engdahl, E.R., Denlinger, R., 1996. Intraslab earthquakes and arc volcanism: dual physical expressions of crustal and uppermost mantle metamorphism in subducting slabs. In: process and deep earthquakes, In: Subduction: Top to Bottom, Am. Geophys. Un. Geophys. Monogr., Vol. 96, pp. 195–214.

Lay, T., 1995. Slab burial grounds. Nature 374, 1154–1156.

Louat, R., Hamburger, M., Monzier, M., 1988. Shallow and intermediate-depth seismicity in the New Hebrides arc: constraints on the subduction process. In: Greene, H.G., Wong, F.L. (Eds.), Geology and Offshore Resources of Pacific Islands—Vanuatu Region. Circum-Pac. Counc. Energy Miner. Resour., Houston, Earth Series, Vol. 8, pp. 329–356.

Lundgren, P.R., Giardini, D., 1994. Isolated deep earthquakes and the fate of subduction in the mantle. J. Geophys. Res. 99, 15833–15842.

Malahoff, A., Feden, R.H., Fleming, H.S., 1982. Magnetic anomalies and tectonic fabric of marginal basins North of New Zealand. J. Geophys. Res. 87, 4109–4125.

McCaffrey, R., 1994. Global variability in subduction thrust zone—forearc systems. Pure Appl. Geophys. 142, 173–224.

Minster, J.B., Jordan, T.H., Molnar, P., Haines, E., 1974. Numerical modelling of instantaneous plate tectonics. Geophys. J. Roy. Astr. Soc. 36, 541–576.

Molnar, P., Freedman, D., Shih, J.S.F., 1979. Lengths of intermediate and deep seismic zones and temperatures in downgoing slabs of lithosphere. Geophys. J. Roy. Astr. Soc. 56, 41–54.

Okal, E.A., 1997. A reassessment of the deep Fiji earthquake of 26 May 1932. Tectonophysics 275, 313–329.

Okal, E.A., Bina, C.R., 1998. On the cessation of seismicity at the base of the transition zone. J. Seismology 2, 65–86.

Okal, E.A., Kirby, S.H., 1995. Frequency-moment distribution of deep earthquakes: implications for the seismogenic zone at the bottom of slabs. Phys. Earth Planet. Inter. 92, 169–187.

Okal, E.A., Talandier, J., 1997. T waves from the great 1994 Bolivian deep earthquake in relation to channeling of S wave energy up the slab. J. Geophys. Res. 102, 27421–27437.

Okal, E.A., Engdahl, E.R., Kirby, S.H., Huang, W.-C., 1995. Earthquake relocations in the Kuril slab: was the 1990 Sakhalin event not isolated after all?. Eos, Trans. Am. Geophys. Un. 76 (17), S199, [abstract].

Parson, L.M., Hawkins, J.W., 1994. Two-stage ridge propagation and the geological history of the Lau back-arc Basin. Proc. Ocean Drilling Prog., Sci. Res. 135, 819–828.

Parson, L.M., Pearce, J.A., Murton, B.J., Hodkinson, R.A., RRS *Charles Darwin* Scientific Party, 1990. Role of ridge jumps and ridge propagation in the tectonic evolution of the Lau back-arc basin, Southwest Pacific. Geology 18, 470–473.

Peterschmitt, E., 1956. Quelques données nouvelles sur les séismes profonds de la Mer Tyrrhénienne. Ann. Geofis. (Roma) 9, 305–334.

Rees, B.A., Okal, E.A., 1987. The depth of the deepest historical earthquakes. Pure Appl. Geophys. 125, 699–715.

Richards, M.A., Wicks, C.W., 1990. $S-P$ conversion from the transition zone beneath Tonga and the nature of the 670 km discontinuity. Geophys. J. Int. 101, 1–35.

Richter, F.M., 1979. Focal mechanisms and seismic energy release of deep and intermediate earthquakes in the Tonga–Kermadec region, and their bearing on the depth extent of mantle flow. J. Geophys. Res. 84, 6783–6795.

Sacks, I.S., 1969. Distribution of absorption of shear waves in South America and its tectonic significance. Carnegie Inst. Wash. Yearb. 67, 339–344.

Silver, P.G., Beck, S.L., Wallace, T.C., Myers, S.C., James, D.E., Kuehnel, R., 1995. Rupture characteristics of the deep Bolivian earthquake of 9 June 1994. Science 268, 69–73.

Smith, W.H.F., Sandwell, D.T., 1997. Global sea floor topography from satellite altimetry and ship depth soundings. Science 277, 1956–1962.

Stark, P.B., Frohlich, C., 1985. The depths of the deepest deep earthquakes. J. Geophys. Res. 90, 1859–1869.

Stein, S., Stein, C., 1996. Thermo-mechanical evolution of oceanic lithosphere: implications for the subduction process and deep earthquakes. **In:** Subduction: Top to Bottom. Am. Geophys. Un. Geophys. Monogr. 96, 1–17.

Sykes, L.R., 1964. Deep-focus earthquakes in the New Hebrides region. J. Geophys. Res. 69, 5353–5355.

Van der Hilst, R., 1995. Complex morphology of subducted lithosphere in the mantle beneath the Tonga trench. Nature 374, 154–157.

Van der Hilst, R.D., Seno, T., 1993. Effects of relative plate motions on the deep structure and penetration depth of slabs below the Izu–Bonin and Mariana island arcs. Earth Planet. Sci. Lett. 120, 395–407.

Van der Hilst, R., Engdahl, E.R., Spakman, W., Nolet, G., 1991. Tomographic imaging of subducted lithosphere below Northwest Pacific island arcs. Nature 353, 37–43.

Van der Hilst, R., Engdahl, E.R., Spakman, W., 1993. Tomographic inversion of P and pP for aspheric mantle structure below the Northwest Pacific region. Geophys. J. Roy. Astr. Soc. 115, 264–302.

von Stackelberg, U., von Rad, U., 1990. Geological evolution and hydrothermal activity in the Lau and North Fiji Basins (SONNE Cruise SO-35)—a synthesis. Geol. Jahrb. D 92, 629–660.

Vassiliou, M.S., Hager, B.H., 1988. Subduction zone earthquakes and stress in slabs. Pure Appl. Geophys. 128, 547–624.

Widiyantoro, S., Van der Hilst, R., 1996. Structure and subduction of lithospheric slab beneath the Sunda Arc. Science 271, 1566–1570.

Wiedicke, M., Collier, J., 1993. Morphology of the Valu Fa spreading ridge in the Southern Lau Basin. J. Geophys. Res. 98, 11769–11782.

Wysession, M.E., Okal, E.A., Miller, K.L., 1991. Intraplate seismicity of the Pacific Basin, 1913–1988. Pure Appl. Geophys. 135, 261–359.

Yan, C.Y., Kroenke, L.W., 1993. A plate tectonic reconstruction of the Southwest Pacific, 0–100 Ma. Proc. Ocean Drilling Prog., Sci. Results 130, 697–709.

Zhou, H.-W., 1988. How well can we resolve the deep seismic slab with seismic tomography?. Geophys. Res. Lett. 15, 1425–1428.